OPENQUATERNARY

Nelson, AR, et al. 2020. Identifying the Greatest Earthquakes of the Past 2000 Years at the Nehalem River Estuary, Northern Oregon Coast, USA. *Open Quaternary*, 6: 2, pp. 1–30. DOI: https://doi.org/10.5334/oq.70

RESEARCH PAPER

Identifying the Greatest Earthquakes of the Past 2000 Years at the Nehalem River Estuary, Northern Oregon Coast, USA

Alan R. Nelson[*], Andrea D. Hawkes[†], Yuki Sawai[‡], Simon E. Engelhart[§], Rob Witter[‖], Wendy C. Grant-Walter[¶], Lee-Ann Bradley[*], Tina Dura[**], Niamh Cahill[††] and Ben Horton[‡‡,§§]

We infer a history of three great megathrust earthquakes during the past 2000 years at the Nehalem River estuary based on the lateral extent of sharp (≤3 mm) peat-mud stratigraphic contacts in cores and outcrops, coseismic subsidence as interpreted from fossil diatom assemblages and reconstructed with foraminiferal assemblages using a Bayesian transfer function, and regional correlation of ^{14}C-modeled ages for the times of subsidence. A subsidence contact from 1700 CE (contact A), sometimes overlain by tsunami-deposited sand, can be traced over distances of 7 km. Contacts B and D, which record subsidence during two earlier megathrust earthquakes, are much less extensive but are traced across a 700-m by 270-m tidal marsh. Although some other Cascadia studies report evidence for an earthquake between contacts B and D, our lack of extensive evidence for such an earthquake may result from the complexities of preserving identifiable evidence of it in the rapidly shifting shoreline environments of the lower river and bay. Ages (95% intervals) and subsidence for contacts are: A, 1700 CE (1.1 ± 0.5 m); B, 942–764 cal a BP (0.7 ± 0.4 m and 1.0 m ± 0.4 m); and D, 1568–1361 cal a BP (1.0 m ± 0.4 m). Comparisons of contact subsidence and the degree of overlap of their modeled ages with ages for other Cascadia sites are consistent with megathrust ruptures many hundreds of kilometers long. But these data cannot conclusively distinguish among different types or lengths of ruptures recorded by the three great earthquake contacts at the Nehalem River estuary.

Keywords: paleoseismology; Cascadia subduction zone; tidal foraminifera and diatoms; coseismic subsidence; Bayesian transfer function; sea-level changes; salt-marsh stratigraphy; earthquake hazards

Introduction

Although coastal wetlands of the Cascadia subduction zone, from British Columbia to northern California (**Figure 1**), host one of the longest and best-preserved onshore records of great (magnitude 8–9) megathrust earthquakes and accompanying tsunamis (e.g., Atwater 1992; Nelson, Shennan & Long 1996; Clague 1997; Witter, Kelsey & Hemphill-Haley 2003; Dura et al. 2016a), debate continues as to the rupture lengths, locations, magnitudes, and timing of Cascadia's megathrust earthquakes (Witter et al. 2012; Atwater et al. 2014; Goldfinger et al. 2016; Hutchinson and Clague 2017). Stratigraphic sequences beneath the coastal wetlands show sharp peat-mud (mud sharply overlying peat) contacts formed by sudden relative sea-level (RSL) rise due to coseismic subsidence during the earthquakes (Atwater 1987; Nelson, Shennan & Long 1996; Milker et al. 2016). The 4–7 sharp peat-mud contacts with 2–3 overlying tsunamis deposits in 3500 years attributed to subsidence along the coasts of northern Oregon and southern Washington, and 12 sharp con-

* Geologic Hazards Science Center, U.S. Geological Survey, Golden, Colorado, US

† Department of Earth and Ocean Sciences, University of North Carolina Wilmington, Wilmington, North Carolina, US

‡ National Institute of Advanced Industrial Science and Technology, Tsukuba, JP

§ Department of Geography, Durham University, Durham, UK

‖ Alaska Science Center, U.S. Geological Survey, Anchorage, Alaska, US

¶ Harwich Port, MA, US

** Department of Geosciences, Virginia Tech, Blacksburg, Virginia, US

†† Department of Mathematics and Statistics, Maynooth University, Kildare, IE

‡‡ Asian School of the Environment, Nanyang Technological University, SG

§§ Earth Observatory of Singapore, Nanyang Technological University, SG

Corresponding author: Alan R. Nelson (anelson@usgs.gov)

tacts and 3–11 tsunami deposits in central and southern Oregon from the past 6300 years, suggest differences in great earthquake history that imply differences in the type and frequency of great earthquakes in different parts of the subduction zone (Nelson 1992a; Nelson and Personius 1996; Kelsey, Witter & Hemphill-Haley 2002; Kelsey et al. 2005; Nelson, Kelsey & Witter 2006; Schlichting and Peterson 2006; Witter et al. 2009; Witter et al. 2013). Offshore, Goldfinger et al. (2012, 2016) interpret a 10,000 year record of turbidites in marine cores as recording strong shaking from great earthquakes (**Figure 1**), with a frequency of about 500 years in northern Cascadia versus a frequency of 200–300 years off southern Oregon and northern California.

The north-to-south contrast in numbers and recurrence of great megathrust earthquakes in land and marine records suggests differences in earthquake history critical to the assessment of earthquake hazard in central western North America, and of tsunami hazard assessment in the Pacific basin. But studies of earthquake or tsunami stratigraphy at many sites at Cascadia are reconnaissance investigations completed 15–30 years ago; few address thresholds for creating and preserving stratigraphic evidence of earthquakes and their tsunamis (e.g., Nelson, Jennings & Kashima 1996; Atwater and Hemphill-Haley 1997; Shennan et al. 1998; Hutchinson et al. 2000; Nelson, Kelsey & Witter 2006; Graehl et al. 2014; Shennan, Garrett & Barlow 2016); and even fewer quantitatively assess deformation during individual earthquakes (e.g., Nelson et al. 2008; Hawkes et al. 2011; Wang et al. 2013; Kemp et al. 2018; Padgett 2019), or use rigorous sample evaluation criteria with statistically based models

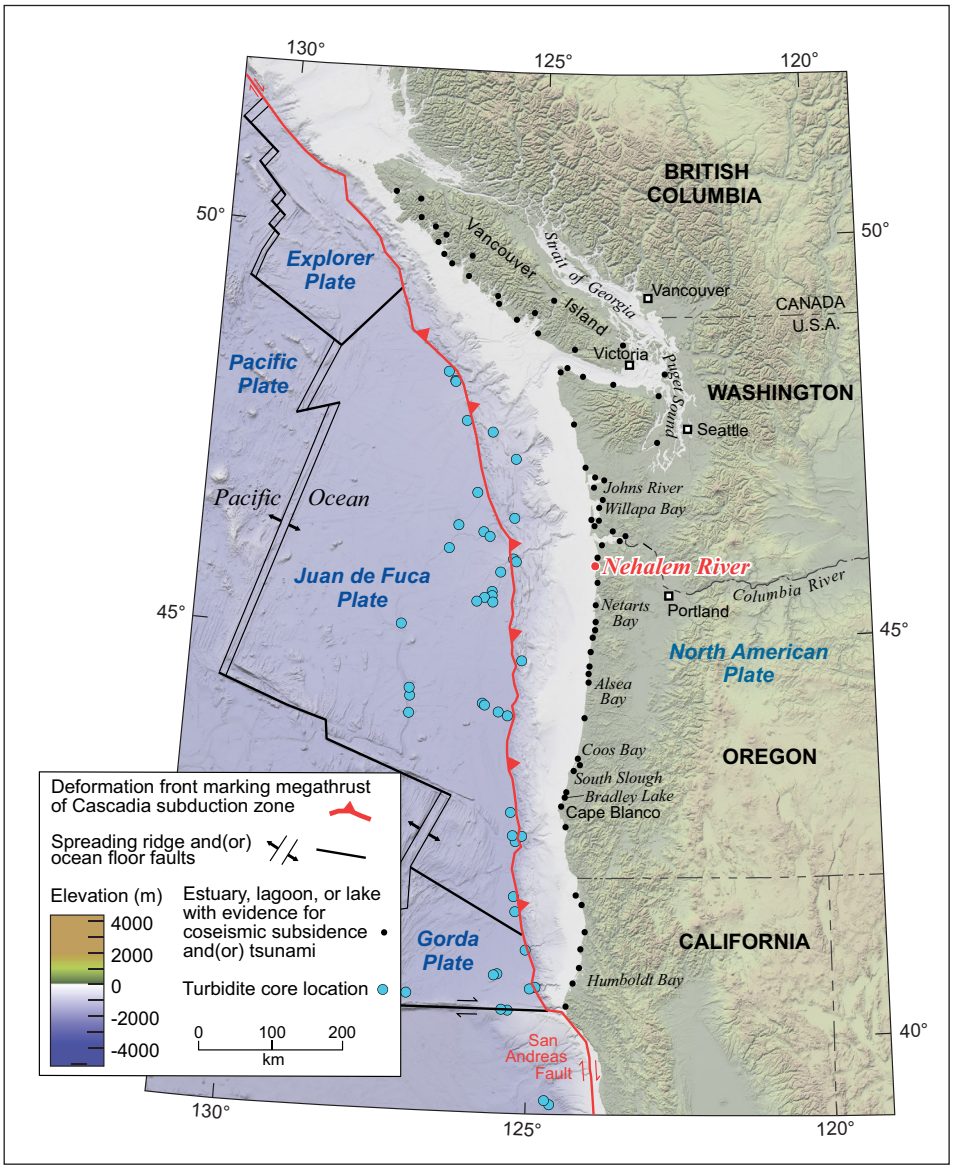

Figure 1: Physiography and major features of the Cascadia subduction zone showing the location of the Nehalem River estuary on the northern Oregon coast (base map data source: GEBCO Compilation Group (2019) GEBCO 2019 Grid, doi:10.5285/836f016a-33be-6ddc-e053-6c86abc0788e). The deformation front of the subduction-zone megathrust fault on the ocean floor (red barbed line) is near the bathymetric boundary between the continental slope and abyssal plain. Dots mark estuaries, lagoons, or lakes with evidence for coastal subsidence, tsunamis, and/or turbidites accompanying subduction-zone earthquakes.

of precise ages to reconstruct earthquake chronology (e.g., Atwater et al. 2004; Witter et al. 2012; Milker et al. 2016; Hutchinson and Clague 2017). Although the investigation summarized here reconstructs the earthquake history of only a single estuary, and so cannot address north-south differences, only through a series of such investigations that employ the above thorough stratigraphic methods at widely spaced sites can we hope to answer questions about north-south differences in earthquake history at Cascadia.

In this paper, we compile and interpret extensive but unintegrated stratigraphic data—collected intermittently over three decades—to reconstruct earthquake history for a key site in the northern Oregon part of the central Cascadia subduction zone. The Nehalem River estuary lies between coastal wetland sites in southwest Washington with thick-mud, thin-peat stratigraphy and fossils suggesting >1–1.5 m of sudden subsidence during great earthquakes (e.g., Hemphill-Haley 1995; Shennan et al. 1996; Atwater and Hemphill-Haley 1997; Kemp et al. 2018), and estuarine sites to the south where thin-mud, thick-peat stratigraphy and microfossil reconstructions suggest a history of substantially less earthquake subsidence (e.g., Nelson 1992; Nelson and Personius 1996; Shennan et al. 1998; Nelson et al. 2008; Wang et al. 2013; Kemp et al. 2018; Padgett 2019) (**Figures 1** and **2**). Based on the initial work of Grant (unpublished 1994 report in Supplementary Files) describing evidence for four megathrust earthquakes in river outcrops, we hoped that Nehalem River estuary stratigraphy would help show how these apparent differences in deformation history transition from north to south. And, by developing more precise age models for

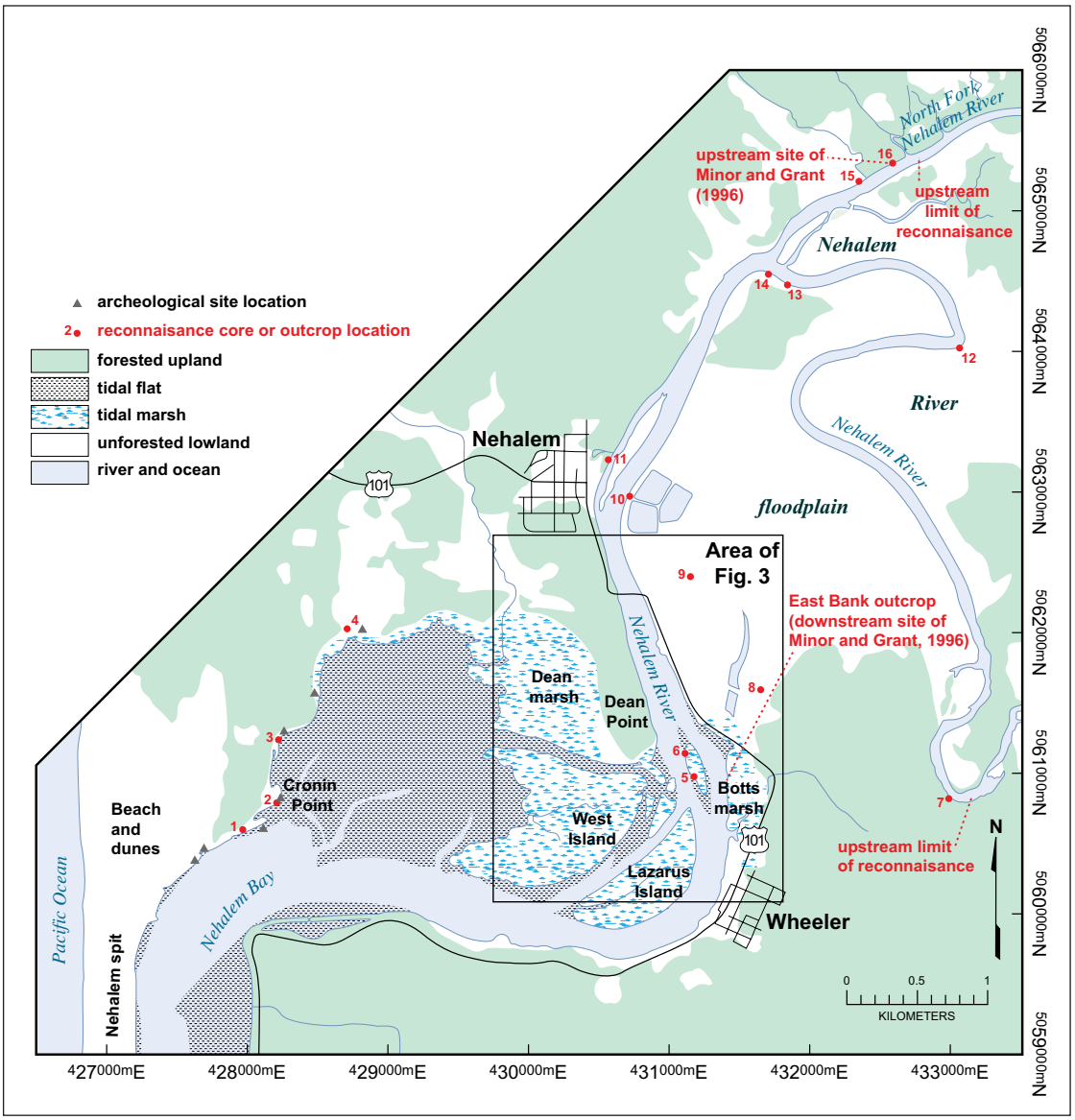

Figure 2: Map of lower Nehalem River valley showing physiographic features, place names, and locations of reconnaissance examinations of cores and outcrops (numbered for reference in text; UTM Zone 10T E coordinates in meters). Cores at locations 1–4 were described by Grant and McLaren (1987), which are close to four archeological sites whose stratigraphy was summarized by Woodward, White & Cummings (1990) and Losey (2002). Minor and Grant (1996) described stratigraphy at their upstream (location 16) and downstream (East Bank outcrop) sites. Figure 3 shows locations of 192 other cores.

the times of earthquakes at the Nehalem River estuary, we sought to test inferences of previous studies about four megathrust earthquake ruptures extending from southwestern Washington into central Oregon in the past 2000 years.

However, in this estuarine lowland with an abundant sediment supply, we found conclusive evidence—widespread, distinct stratigraphic contacts marking substantial coseismic subsidence—for only three megathrust earthquakes in the past 2000 years. Foraminiferal and diatom microfossil analyses help us identify significant environmental change across the peat-mud (mud-over-peat) subsidence contacts. Using new Bayesian statistical methods with the foraminiferal data we measure 0.7 to 1.1 m of subsidence during the three earthquakes. Age models of the results of our ^{14}C ages on plant macrofossils, although they date contacts more precisely, demonstrate ongoing uncertainties in correlating lithologic and microfossil evidence of earthquakes, even over hundreds of meters at the same site, as well as among sites hundreds of kilometers apart along the subduction zone (e.g., Shennan, Garrett & Barlow 2016). Next, we summarize our approach to evaluating potential earthquake contacts prior to discussing the stratigraphy and correlation of contacts.

Approach and Methods

Mapping potential earthquake contacts

In outcrops and cores of the lower Nehalem River estuary, we followed many previous studies of Cascadia earthquake stratigraphy at tidal sites by mapping sharp (defined as ≤3 mm to ≤10 mm, depending on the study) to abrupt (≤1 mm) peat-mud or peat-sand contacts between the peaty sediment of marshes or swamps (O or A soil horizons) overlain by muddy or sandy tidal-flat sediment, which potentially mark sudden coastal subsidence during great earthquakes commonly followed by tsunamis. Successions of similar mud-peat couplets (mud grading upward into peaty mud and peat) with sharp upper contacts are the stratigraphic basis for interpretations of repeated sudden subsidence of wetlands during great Cascadia earthquakes at tens of tidal sites along the subduction zone (e.g., Atwater 1992; Nelson 1992b; Darienzo, Peterson & Clough 1994; Nelson, Jennings & Kashima 1996; Schlichting and Peterson 2006; Valentine et al. 2012; Graehl et al 2014; Milker et al. 2016), and on other subduction-zone coasts (e.g., Briggs et al. 2014; Shennan et al. 2014; Dura et al. 2016a). In evaluating earthquake evidence at Nehalem we apply the following stratigraphic criteria of Nelson, Shennan & Long (1996), as modified by and best articulated by Shennan, Garrett & Barlow (2016): (1) lateral extent of sharp peat-mud contacts; (2) suddenness of submergence; (3) amount of submergence, quantified with errors; (4) synchroneity of submergence based on statistical age modelling; (5) spatial pattern of submergence; and 6) additional evidence, such as of a tsunami concurrent with submergence.

In our mapping of evidence for great Cascadia earthquakes and accompanying tsunamis we compiled and interpreted data from field investigations decades apart (primarily in 1987–1992 and 2006–2010) in the lower valley of the Nehalem River and adjacent areas of Nehalem Bay (**Figure 2**). Grant and McLaren (1987), Grant (1989), and Grant (unpublished 1994 report in Supplementary Files) described shallow (<2 m depth) stratigraphy in about 120 gouge (2.5 cm diameter) cores and 6 outcrops near the river and along the northern parts of the bay (**Figures 2** and **3**). Stratigraphic sequences with four sharp peat-mud contacts at two outcrops (mapped by Grant at the tops of organic-rich, wetland soil O or A horizons) were described in greater detail and dated with 29 radiocarbon ages (Grant et al. 1989; Grant, unpublished 1994 report in Supplementary Files; Minor and Grant 1996; **Table 1**). In 2006, we identified the three youngest peat-mud contacts in the East Bank outcrop (**Figures 2** and **3**; "downstream" site of Grant, unpublished 1994 report in Supplementary Files; **Table 1**), but silty mud deposited against the outcrop—perhaps a result of cessation of dredging the main river channel—had reduced its (1991) height by >1 m. Because the outcrop was longer and higher in 1991 than in 2006, we adopted Grant's (unpublished 1994 report in Supplementary Files, her **Figure 7**) mapping of the four peat-mud contacts, labeling them A, B, C, and D (**Figures 4** and **5**).

To obtain a more complete section of the East Bank outcrop stratigraphy, in 2006 we took four 4-m-long vibracores (70-mm diameter, labeled V1–V4) on the dike above the outcrop 3–4 m from its eroded edge (**Figure 4**). Cores were split, cleaned, and photographed the following day. In the laboratory we described the lithostratigraphy of core V1 and recorded its lithology with the locations of microfossil and ^{14}C samples on a color-corrected, photo mosaic of the core (methods of Troels-Smith 1955, and Nelson 2015). Although core V1 compacted 12% during collection, we approximately corrected its contact depths through correlations to adjacent less compacted gouge cores (**Figures 5**, S1, and S2). Short sections of cores V3 and V4 spanning peat-mud contacts were saved only for ^{14}C sampling.

Investigations in 2009 included reconnaissance examination of river outcrops; reconnaissance description of cores in tidal marshes west of the river, along the northern edge of Nehalem Bay, and in pastures north of Highway 101; further laboratory study of vibracores at the East Bank outcrop; and description, correlation, and dating of gouge and Russian (segments 50 cm long with 5-cm diameter, D-shaped cross-sections) cores in Botts marsh east of the East Bank outcrop (**Figures 2, 3, 5**, and S2). In 2018, we dated and studied foraminifera across the lower four of five peat-mud contacts in Russian core R5 from Botts marsh. We used a Real Time Kinematic-Global Positioning System (RTK-GPS) to measure core and sample elevations using standard methods (described in the Supplementary Files).

Dating earthquake contacts through ^{14}C-age modeling

Following Grant's (Grant et al. 1989; unpublished 1994 report in Supplementary Files) reasoning for dating materials above and below contacts, we used previous ^{14}C ages or selected new ^{14}C samples based on our assessment of how close the age of sample materials (either maximum

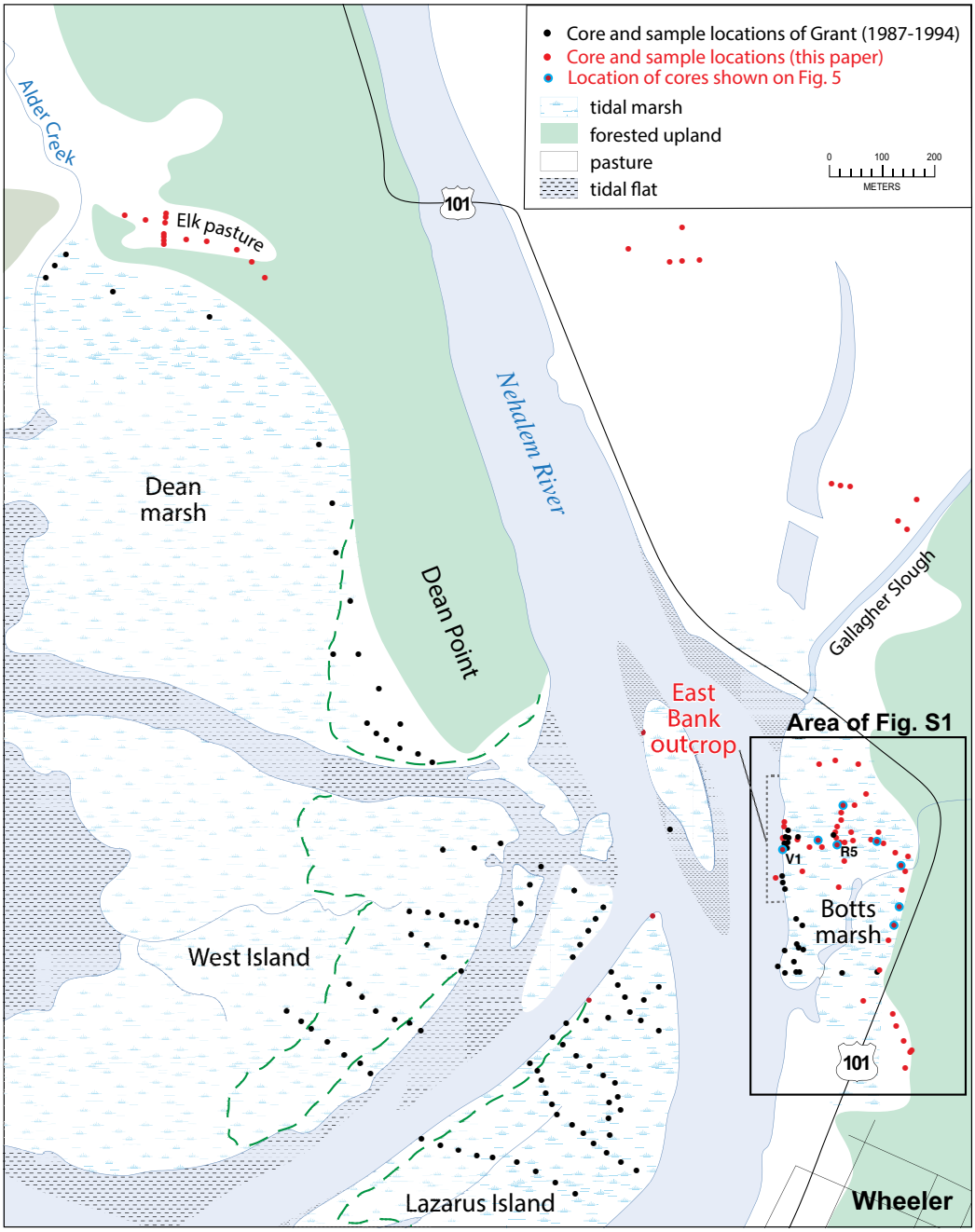

Figure 3: Map of areas of tidal marsh, meadow, and pasture in the lower Nehalem River valley where most of the cores in this study were described. Black dots show locations of gouge cores and a few sampled outcrops of Grant and McLaren (1987) and Grant (1989; unpublished 1994 report in Supplementary Files). Red dots show locations of gouge cores and outcrops examined in this study (2006–2009). Red dots with blue rings show locations of cores (V1 and R5 labeled) selected for Figure 5 from west to east. Areas of marsh are taken from a 1979 U.S. Geological Survey quadrangle map (Nehalem River, Oregon; 1:100k) and because of recent changes in the position of marshes and tidal flats, cores taken in tidal marshes in 1987–2009 do not all fall on the depicted areas of marsh. Approximate edges of marshes west of the river as surveyed by Gilbert (1875) are shown by green dashed lines. Locations of labeled cores in Botts marsh are shown on imagery in Figure S2.

or minimum ages) were to the times when the four contacts at the East Bank outcrop formed (**Table 1**). Previous ages included: 13 liquid-scintillation ^{14}C ages on Sitka spruce (*Picea stitchensis*) stump roots, peat, rooted herb (*Triglochin maritima)* rhizomes, and detrital sticks and bark (Grant, unpublished 1994 report in Supplementary Files, her **Table 1**); Nelson et al.'s (1995) eight accelerator mass spectrometry (AMS) ^{14}C ages and four high-precision gas-proportional ^{14}C ages on rooted herbs and stumps at contact A; two AMS ages on a fragment of a Native American basket at contact A, twelve AMS ages on plant macrofossils from cores V1–V4, and two AMS ages on needles and a cone in forest litter beneath stumps exposed on the present tidal flat (**Table 1; Figures 4** and **5**). To extend correlations with contacts in the East Bank outcrop eastward across Botts marsh (**Figures 2, 3, 5**, S1, S2, and S3)

Table 1: Radiocarbon data for samples from the East Bank outcrop and from cores in Botts marsh at Nehalem River[a].

Calibrated age (cal a BP at 95% CI)[b]	Lab-reported age (^{14}C a BP at 1s)[c]	Provenance interpretation[d]	Radiocarbon lab no.	Core/ exposure[e]	Depth (m)[f]	Description of dated material
East Bank outcrop (unpublished 1994 report in Supplementary Files; Minor and Grant, 1996)						
Contact A **1700 CE (assumed) 269–15**	110 ± 60	minimum	Beta-27867	NR112A a	1.17	Rhizomes of *Triglochin maritima* in mud 15 cm above contact A
	260 ± 65	minimum?	Beta-23210	NR77A b	1.15	Rhizomes of *Triglochin maritima* in mud 5 cm above contact A; 55 m south of outcrop in Fig. 4
	128 ± 9	**within yrs**	QL (see notes)	E6, E7, E8	1.25	Average of 3 ages on outer 1–10 rings cut from roots of *Picea sitchensis* and cf. *Pyrus fusca* stumps at contact A
	211 ± 13	within yrs	QL-4643	E8	1.25	Rings 39–41 cut from E8 root of *Picea sitchensis* stump at contact A
	179 ± 15	**within yrs**	GX (see notes)	E c	1.12	Leaf bases and subaerial stems of *Argentina egedii* and *Juncus* cf. *J. arcticus* rooted in top of peaty unit at contact A
	130 ± 60	minimum?	Beta-27871	NR114A d	1.20	Upper 3 cm of peat beneath contact A; sample may have included younger rootlets
	170 ± 60	maximum	Beta-31818	NR122A e	1.04	*Picea sitchensis* root in peaty unit
	176 ± 45	maximum	GX-17835	E f	1.25	Fragment of a woven basket of cedar bark horizontal in mud 1 cm above contact A
	290 ± 90	maximum	Beta-27874	NR114C1 g	1.22	Sticks from peaty unit 3 cm below contact A
	350 ± 50	maximum	Beta-27875	NR114C2 h	1.22	Fragment of bark from peaty unit 3 cm below contact A
Contact B **942–764**	630 ± 70	minimum	Beta-23211	NR77C i	2.01	Growth position rhizomes of *Triglochin maritima* in mud 5 cm above contact B, 55 m south of outcrop in Fig. 4
	790 ± 70	minimum	Beta-45951	NR130A j	2.01	Growth position rhizomes of *Triglochin maritima* in mud 5 cm above contact B
	880 ± 30	minimum	OS-72603	V1 k	1.99	Matted stems or leaves attached to herb rhizome, probably *Carex* sp., in mud 5 mm above contact B
	900 ± 30	minimum?	OS-62143	V4 l	1.75	Herb rhizome, possibly *Carex* sp, retained on sieve in mud ~10 cm above contact B
	970 ± 50	**minimum**	Beta-45952	NR130A2 n	2.04	Growth position rhizomes of *Triglochin maritima* in mud 2 cm above contact B
	940 ± 45	**maximum**	OS-62290	V3 m	1.96	3 fragments of abraded wood and 1 *Picea sitchensis* needle from muddy peat 1–2 cm below contact B
	980 ± 35	**maximum?**	OS-72602	V1 o	2.00	Horizontal woody herb rhizome at top of muddy peat at contact B

(Contd.)

Calibrated age (cal a BP at 95% CI)[b]	Lab-reported age (^{14}C a BP at 1s)[c]	Provenance interpretation[d]	Radiocarbon lab no.	Core/ exposure[e]	Depth (m)[f]	Description of dated material
Contact C (at outcrop) **1119–915**	**1160 ± 80***	**minimum**	Beta-45954	NR130B r	2.36	Growth position rhizomes of *Triglochin maritima* in mud 2 cm above contact C
level x (samples from depths in vibracores similar to Contact C in outcrop) **1180–1065**	**1200 ± 25**	**minimum**	OS-62148	V4 p	2.00	Growth position rhizome and leaves of herb, probably *Carex* sp., in peaty mud
	1200 ± 30	**minimum**	OS-62118	V3 q	2.21	Stem base and leaf bases of *Triglochin maritima* in sandy peaty mud
	1190 ± 30	**maximum**	OS-62292	V4 s	2.35	15 fragments of leaf (cf. *Gaultheria shallon*), 5 stems of *Fontinalis* sp. from upper 4 cm of peaty mud
	1190 ± 30	**maximum**	OS-62291	V4 t	2.35	28 fragments of *Picea stitchensis, Tsuga mertensiana, Thuja plicata* needles from upper 4 cm of peaty mud
	1260 ± 35	maximum	OS-62093	V4 u	2.35	Black, knobby, herb rhizome from upper 4 cm of peaty mud
	1310 ± 35	maximum	OS-62518	V4 v	2.35	Deciduous twig from upper 4 cm of peaty mud
Contact D **1681–1244**	1970 ± 60	OxCal outlier	Beta-27868	NR113A z	2.52	Rhizomes of *Triglochin maritima* in mud 20 cm above contact D; inconsistent with other ages at same stratigraphic level
	1690 ± 30	**maximum**	OS-75680	T09B w	2.9	Bracts from 3-cm-long *Picea sitchensis* cone in top of peaty AO horizon at contact D
	1700 ± 60	maximum	Beta-27870	NR113C2 x	2.77	Piece of stump of *Picea sitchensis* in growth position in peat below contact D
	1740 ± 40	maximum	OS-75679	T09A y	2.9	10 *Picea sitchensis* needles in mud 3 mm above contact D
	2060 ± 80	OxCal outlier	Beta-27869	NR113B aa	2.77	Piece of stump of *Picea sitchensis* in growth position in peat below contact D
Below stumps	1290 ± 35	OxCal outlier	OS-72604	V1 bb	3.91	Detrital stems of the aquatic moss *Frontinalis* sp.
	1310 ± 35	OxCal outlier	OS-72605	V1 cc	3.91	Detrital fragments of deciduous leaves, possibly *Gaultheria shallon*
Botts Marsh cores						
Contact A **1700 CE** (assumed) **290–125**	**190 ± 25**	**maximum**	OS-127134	R17	0.81	22-mm-long piece of stem lining or inner bark horizontal in mud 1 cm above contact A
	445 ± 25	maximum	OS-101394	R24	0.86	4 seeds: 1 large *Schoenoplectus* sp., 1 broken *Atriplex*-type, and 2 others from muddy peat 2–4 cm below contact A

(Contd.)

Calibrated age (cal a BP at 95% CI)[b]	Lab-reported age (^{14}C a BP at 1s)[c]	Provenance interpretation[d]	Radiocarbon lab no.	Core/ exposure[e]	Depth (m)[f]	Description of dated material
level z (indistinct contact) **706–363**	**725 ± 20**	**maximum**	OS-144142	R5	1.42	Detrital *Atriplex* seed, *Picea sitchensis* needle, and unidentified seed in peaty mud 1–3 cm above faint contact
	760 ± 20	**maximum**	OS-144143	R5	1.50	Growth position stem base of *Triglochin maritima* in peat 6 cm below faint contact
	830 ± 15	maximum	OS-144344	R5	1.68	Growth position stem base of *Triglochin maritima* in muddy peat 23 cm below faint contact
Contact B **1017–707**	**855 ± 25**	**minimum?**	OS-144330	R5	2.08	Growth position *Triglochin maritima* rhizome and stem base in muddy peat 4 cm below contact B
	1100 ± 15	**maximum**	OS-144331	R5	2.01	5 fragments of *Picea sitchensis* needles and twig in muddy peat 2–4 cm above contact B
	1670 ± 20	OxCal outlier	OS-144347	R5	2.05	Three fragments of *Picea sitchensis* needles and two seeds from peat 0–2 cm below contact B
Contact D **1568–1361**	**1520 ± 40**	**minimum**	OS-104086	R24	1.77	Growth position *Triglochin maritima* leaf base 1–3 cm above contact D
	1620 ± 40	**maximum**	OS-98634	R24	1.81	3 *Atriplex*-type seeds, 2.5 *Potamogeton*-type seeds from upper 1–3 cm of peat below contact D
	1630 ± 50	**maximum**	OS-98643	R24	1.80	2 *Sphagnum*-type stems and 1 *Fontinalis*-type stem in peaty mud 2–6 cm above contact D
	1700 ± 20	maximum	OS-127133	R17	2.49	2 bracts from *Picea sitchensis* cone horizontal in muddy peat 2 cm below contact D
	1700 ± 20	maximum	OS-144489	R5	2.40	11 cf. Cyperacea sp. seeds in peat 0–2 cm below contact D
	1710 ± 25	maximum?	OS-101244	R24	1.75	Horizontal rhizome, possibly *Carex*-type, 2 cm below contact D
	1710 ± 25	maximum	OS-144488	R5	2.40	10 *Picea sitchensis* needles, horizontal in peat 0–2 cm below contact D
	1740 ± 20	maximum	OS-144487	R5	2.20	Sheaths from detrital woody herb stem in muddy peat 20 cm above contact D
	1810 ± 25	OxCal outlier	OS-98635	R24	1.79	3 *Picea sitchensis* needles in pieces, horizontal in mud 8–9 mm above contact D
	2140 ± 40	OxCal outlier	OS-98642	R24	2.03	3 angular fragments of wood charcoal from peaty bed of wood fragments 1–3 cm below contact D

(Contd.)

Calibrated age (cal a BP at 95% CI)[b]	Lab-reported age (^{14}C a BP at 1s)[c]	Provenance interpretation[d]	Radiocarbon lab no.	Core/ exposure[e]	Depth (m)[f]	Description of dated material
Contact E **1857–1570**	**1840 ± 25**	**maximum**	OS-98636	R17	2.49	1 bract from *Picea sitchensis* cone horizontal in upper 2 cm of peat below contact E
	1860 ± 30	**maximum**	OS-98633	R24	2.25	Half large seed, decayed *Picea sitchensis* needle, 1 seed case, 12 black seed cases from woody peat 2–4 cm below contact E
	1870 ± 25	**maximum**	OS-98641	R24	2.29	3 decayed *Picea sitchensis* needles in pieces from woody muddy peat 5–8 cm below contact E
	1890 ± 20	maximum	OS-144141	R5	2.84	Sheath of herb stem in peaty mud 7 cm below contact E
	1910 ± 20	maximum	OS-144140	R5	2.78	Decayed detrital herb stem in muddy peat 1 cm below contact E
	2010 ± 30	maximum	OS-101243	R24	2.21	9 barrel-shaped seeds, 2.5 seed cases, 1 yellow seed, 1 white seed in peat 0–3 cm below contact E
unconformity	2210 ± 25	maximum	OS-98640	R24	2.37	4 axial harpoons from growth-position woody stems of *Triglochin maritima* 7 cm below peat beneath inferred unconformity

[a] Ages are on plant parts collected above or below sharp upper contacts of peaty units in outcrop and cores (vibracores V1, V3, and V4; and Russian cores R5, R17 and R24; Figs. 4, 5, S1, S2, and S3).

[b] Modeled age (95% CI, confidence interval) for contacts at the top of peaty units based on laboratory-reported ages (in solar years; shown in bold in second column) selected with OxCal sequence analyses (version 4.3; Bronk Ramsey, 2001, 2008; 2009; probability method). For contact A at the East Bank outcrop, only the calibrated age probability distributions for the two most precise ages (averages of multiple ages shown in bold), on plants inferred to have died about the time of the 1700 CE earthquake, are shown. Time intervals for other contacts (time intervals of >95% probability distribution using the INTCAL04 atmospheric dataset of Reimer et al., 2013) were calculated from maximum or minimum ages listed in bold in second column for each contact. As explained in the Supplementary Files for this paper, prior to calibration we increased the errors on laboratory-reported ages (second column): for 20th-century ages as recommended by Taylor, Stuiver & Reimer (1996), for NOSAMS ages by adding 2.6‰ of additional variance to errors for reported modern fractions for each age. In later OxCal sequence analyses, when the laboratory-reported mean ages (rounded to nearest 5 years) of 2–3 maximum or minimum ages were within 40 years of each other, the ages were averaged.

[c] Ages reported by radiocarbon laboratory in solar years on materials in right-most column. Ages with "Beta" laboratory numbers are radiometric liquid-scintillation ages (dry sample weights were between 12 and 57 g). Quoted errors for AMS (accelerator mass spectrometer) ages ("GX-" and "OS-" laboratory numbers) are the larger of counting error or target reproducibility error. The 128 ± 9 ^{14}C a BP age is the mean of three high-precision gas-proportional ages (QL-4640, 4641, and 4642) on roots of three stumps (Fig. 4), as reported in Nelson et al. (1995). The 179 ± 15 ^{14}C a BP age is the mean of 8 AMS ages (GX-17840, 17844, 17929, 17934, 17939, 17944, 17949, and 17954) on eight herbs in growth position at contact A, as explained in Nelson et al. (1995). GX-17835 is the average of two ages on the same basket fragment (Connolly and Byram, 1997; Atwater et al. 2005, p. 21). Liquid-scintillation ages (Beta-) are on samples collected by Grant and Atwater in 1988–1991(Table 1 in Grant, unpublished 1994 report in Supplementary Files). AMS samples labeled "GX-" and high-precision ages labeled "QL-" were collected by Atwater, Nelson, and Grant in 1991, as described in Nelson et al. (1995). Other AMS ages (OS-) collected by Nelson, Hawkes, Witter, and Grandpre, in 2006–07 and Nelson, LaSelle, and Pagette in 2018 weighed 2–45 mg and yielded ^{13}C values between −17.4 and −27.9‰. Ages from this site are also discussed by Minor and Grant (1996). Maximum and minimum ages used in the final OxCal sequence analyses for the outcrop and for cores from Botts marsh (in bold) were selected on the basis of type of material dated (degree of preservation, detrital or growth-position, stratigraphic context) and the results of OxCal outlier analyses (e.g., Bronk Ramsey, 2009).

[d] Interpretation of the provenance, or stratigraphic context, of the dated sample relative to the time sharp contacts formed, which we infer is the result of subsidence during great earthquakes**.** Maximum ages are on samples containing carbon judged to be older than the contact based on information in right-most column; minimum ages are on samples judged younger than the contact; ages labeled "within yrs" are on plants inferred to have died within a few years of the earthquake (Nelson et al. 1995). Ages identified by our initial OxCal age models as outliers using all ages from the East Bank outcrop and from Botts marsh cores are labeled.

[e] E, East Bank outcrop samples collected by Atwater, Nelson, and Grant in 1991; NR, original sample numbers of Grant (1989) (see Fig. 7 and Table 1 in Grant's unpublished 1994 report in Supplementary Files); T09, tidal-flat samples collected by Nelson in 2009; V, vibracore; R, Russian core. Lowercase letter at right locates sample on Fig. 4.

[f] Depths (m) corrected (using contacts A and B as reference points) to match compaction-corrected depths of core V1 and contacts along 160 m of outcrop surveyed by Grant (unpublished 1994 report in Supplementary Files) (Fig. 4).

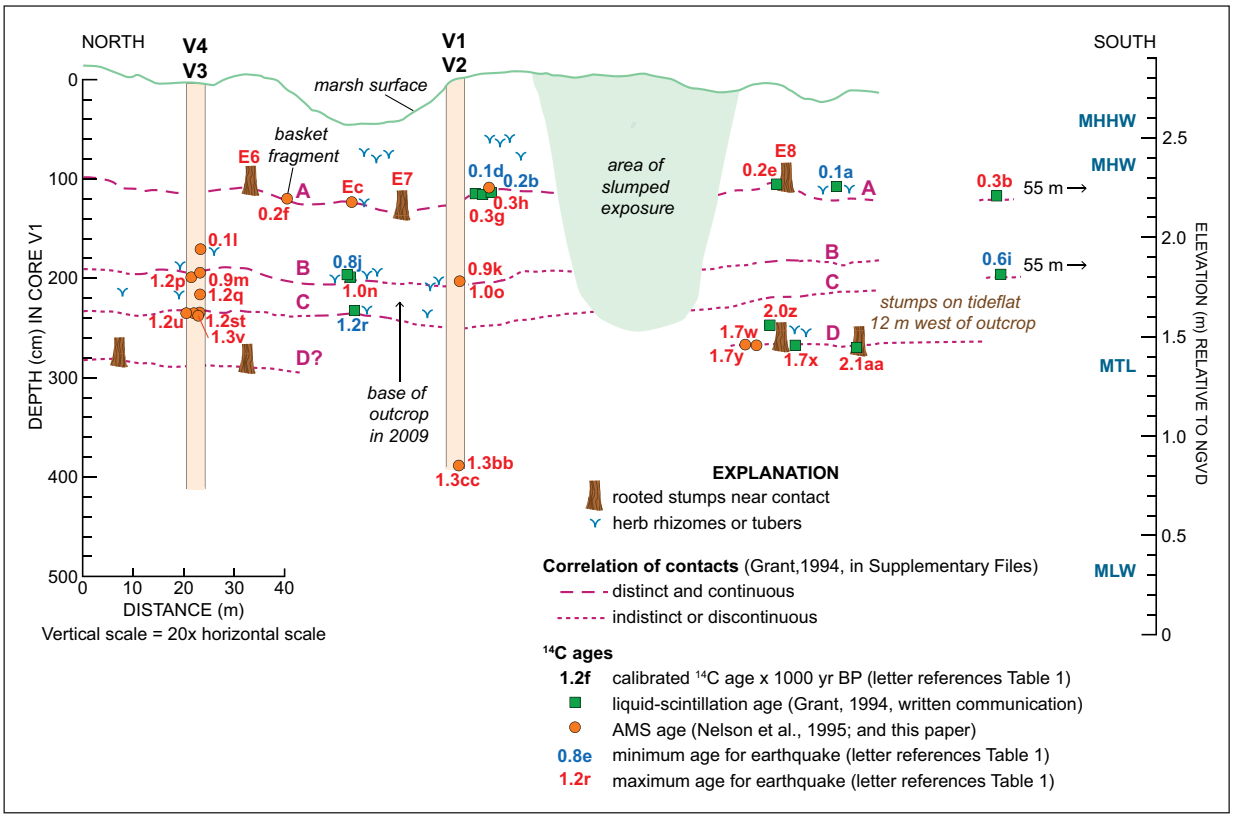

Figure 4: Correlation of peat-mud contacts, mapped and inferred by Grant (1989; modified from Figure 7 in her unpublished 1994 report in Supplementary Files) to mark the upper contacts of marsh O horizons suddenly subsided during great earthquakes, relative to cores and samples from the East Bank outcrop. Vibracores (V1–V4) were collected 3–4 m east of the top of the outcrop (Figure S2). Location, type, and interpretation of ^{14}C ages in Table 1 are also shown. Two liquid-scintillation ages of Grant (Table 1 in unpublished 1994 report in Supplementary Files) are on samples 55 m south of their position shown on the figure. The fragment of a Native American basket, found by Atwater, Grant, and Nelson in 1991, is described by Connolly and Byram (1997). Core elevations measured relative to tide levels (MTL, mean tide level; MHW, mean high water; MLW, mean low water; MHHW, mean higher high water) with kinematic GPS (RTK) relative to NAV88.

we selected plant macrofossils from Russian cores R5, R17, and R24 for AMS ^{14}C dating and prepared them as for vibracore samples (methods of Kemp, Nelson & Horton 2013).

We used OxCal stratigraphic ordering software (methods of Bronk Ramsey 2008, 2009) with the ^{14}C ages to develop age models for the times when peat-mud contacts formed (models similar to those described by DuRoss et al. 2011, and Nelson et al. 2014). Our series of age models begins with outlier analyses (method of Bronk Ramsey 2009) of 1) the 30 ages from the East Bank outcrop, and 2) the 25 ages from Botts marsh (**Table 1; Figure 6**; OxCal code for selected models in Supplementary Files). For each of the two series of models we then successively eliminated ages that we interpret to be less accurate minimum or maximum estimates of the times contacts formed. For our final age models, we selected only the closest maximum and minimum ages for contacts (marked in bold on **Table 1**). Where the two youngest maximum or oldest minimum ages (as reported by laboratories) were within 40 ^{14}C years of each other and met the criteria of Ward and Wilson (1978) for being from the same population (0.05 confidence level), we averaged ages (e.g., Bronk Ramsey 2015).

We base our interpretations of the closest maximum and minimum ages (discussed for each contact below) on the type of plant macrofossil, its orientation, degree of decay and abrasion, host stratigraphic unit lithology, its stratigraphic context relative to adjacent plant macrofossils and to upper and lower units, and—most importantly—on its calibrated ^{14}C age relative to the ages of samples above and below it. As elsewhere in Cascadia coastal sequences (e.g., Nelson 1992b; Nelson et al. 2006; Hutchinson and Clague 2017), most of our ages are on detrital materials, which are older than the times adjacent contacts formed. The relative age of rhizomes (below ground stems) of low and middle marsh herbs are more difficult to interpret than ages on above-ground plant parts. Usually growth-position rhizomes, especially those of *Triglochin maritima* with the bases of its decay-resistant leaves still attached, provide unambiguous minimum ages for underlying contacts. Rarely, we infer that the rhizomes of plants younger than contacts grew down into the peaty unit just below a contact (sample OS-144330, **Table 1**).

Microfossil-based assessments of environmental change across earthquake contacts

Over the past two decades, the use of changes in fossil foraminiferal and diatom assemblages to stratigraphically identify great earthquakes at Cascadia has shifted from

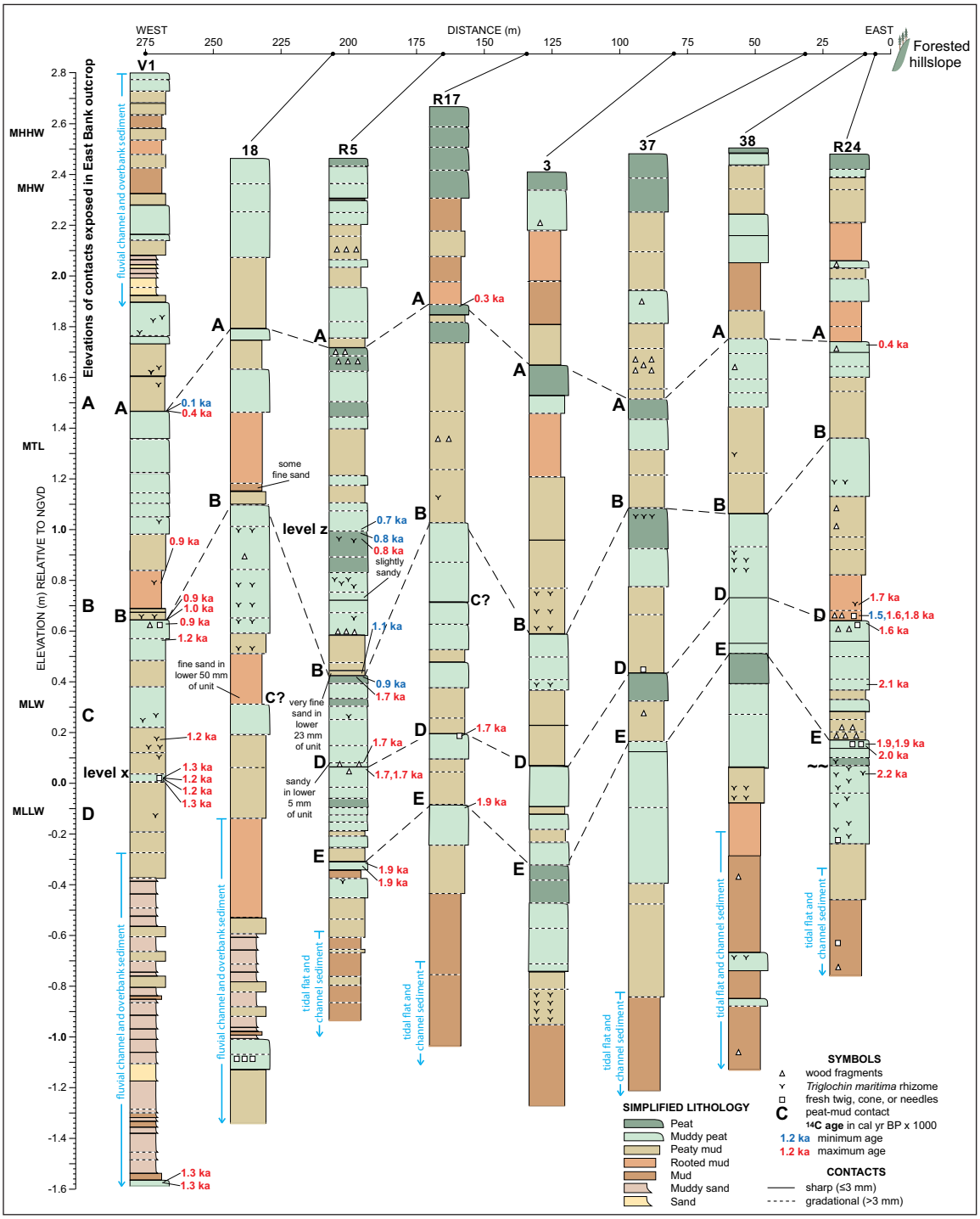

Figure 5: Simplified lithology, correlation of distinct contacts (dashed lines), and ^{14}C ages (median of calibrated probability distribution rounded to century) in selected gouge and other cores (vibracore V1, Russian cores R5, R17, and R24) between the East Bank outcrop and the east edge of Botts marsh (Figures 2, 3, and 4; core locations are highlighted on Figure S2; more detailed correlation of 20 cores in Figures S2 and S3). Upward and lateral changes in lithology are considerably more subtle and variable than suggested by the simplified lithologies. Examples of the more detailed field and laboratory descriptions used in interpreting and correlating cores are shown in Figures S1 and S3. Table 1 lists data for radiocarbon ages. Core elevations measured relative to tide levels with kinematic GPS (RTK) relative to NAV88. Unit thicknesses in core V1 have been approximately corrected for compaction based on key contacts in nearby gouge cores. Contact A is sharp and distinct in almost all cores. Contact B is distinct along the outcrop and in cores in much of the northwestern and northeastern marsh, but its correlation is uncertain in the central marsh. Level x and level z are too indistinct to be considered mappable contacts (discussed in the text). Contact C is mapped along parts of the East Bank outcrop (Figure 4), but possible correlative contacts were found in only 5 cores in Botts marsh. Contact D has been eroded in most cores near the river, but it is sharp and distinct in core R5 and in cores in the central and northeastern marsh. Contact E can be correlated intermittently among two-thirds of the cores that reach its depth in the central and eastern marsh.

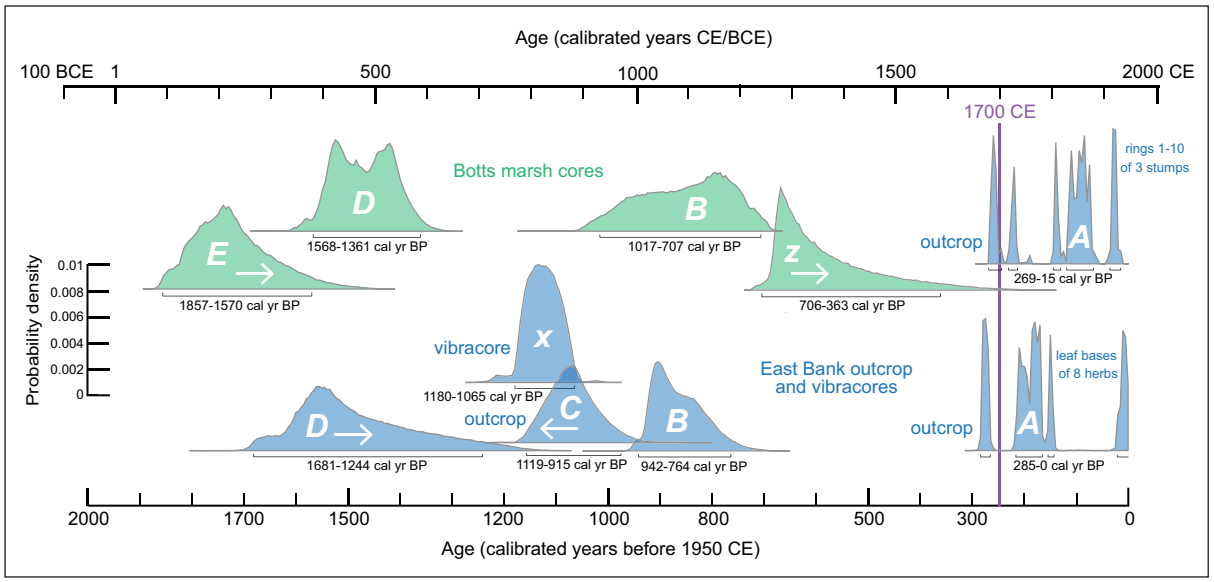

Figure 6: Radiocarbon-age probability distributions for contacts A, B, C, D, and E (and levels x and z; explained in text), at the East Bank outcrop (blue) and(or) Botts marsh (green) determined with OxCal (Bronk Ramsey 2001, 2009). The two distributions for contact A are averages for plants rooted in the peaty O soil horizon just below contact A at the outcrop (Table 1; Figure 4), and inferred to have died about the time of the 1700 CE earthquake. Dated samples consisted of rings 1–10 from each of three tree stumps and the leaf bases of eight herbs (Nelson et al. 1995). Other distributions were determined with age models using maximum-limiting and minimum-limiting ^{14}C ages selected from Table 1. Distributions calculated only with maximum-limiting ages are marked with white right-pointing arrows; with a minimum limiting age with a left-pointing arrow.

using mostly qualitative and limited quantitative comparisons of assemblages to estimate amounts and rates of RSL rise across peat-mud contacts (e.g., Nelson et al. 1996b, 1998; Atwater and Hemphill-Haley 1997; Shennan et al. 1998; Kelsey et al. 2002; Witter, Kelsey & Hemphill-Haley 2003; Hawkes et al. 2005; Graehl et al. 2014) to transfer function methods that produce sample specific errors (e.g., Guilbault, Clague & Lapointe 1995, 1996; Nelson et al. 2008; Hawkes et al. 2011; Wang et al. 2013; Dura et al. 2016b; Milker et al. 2016; Shennan, Garrett & Barlow 2016; Horton et al. 2017). Transfer functions use the relations among modern assemblages and their respective elevations in modern tidal environments as analogs to hindcast past tidal elevations from fossil assemblages in stratigraphic sequences (Kemp and Telford 2015). The most recent development are Bayesian foraminiferal transfer functions (Cahill et al. 2016; Kemp et al. 2018; Hong 2019; Padgett 2019) that, unlike previous non-Bayesian transfer functions, allow species response curves to deviate from a pre-defined form (commonly unimodal) and may incorporate prior information about sampled sediment (i.e., stratigraphy, lithology, paleoecologic information from other types of fossils) to help constrain estimates of past RSL change.

Foraminiferal analysis

At the Nehalem River estuary, a new Bayesian foraminiferal transfer function was used to reconstruct the amount of rapid submergence (inferred to be the result of coseismic subsidence) across potential earthquake contacts (**Figures 4, 7**, and S4; Table S1). Kemp et al. (2018) used the original foraminiferal data of Hawkes et al. (2011; 22 samples) with their new Bayesian transfer function to estimate the amount of subsidence marked by contact A in vibracore core V1 at the East Bank outcrop. Kemp et al. (2018) developed their Bayesian transfer function using a modern dataset of 393 samples and elevations from 19 sites between southern California and Vancouver Island. The much larger dataset than used to develop previous, non-Bayesian functions (e.g., Hawkes et al. 2010; Engelhart et al. 2013a, 2013b; Milker et al. 2015b, 2016) includes modern assemblages that are better analogs for fossil assemblages than those of earlier studies (e.g., Shennan, Garrett & Barlow 2016; Kemp et al. 2018). With the new foraminiferal data reported here (73 samples), we used the same function (informed West Coast function of Kemp et al. 2018) to estimate subsidence across contact B in core V1, and contacts B and D in Russian core R5 from Botts marsh. Insufficient foraminifera or inconsistent results prevented us from estimating subsidence for three other potential earthquake contacts in cores V1 and R5 (Figure S4). Based on the partially contorted sediment of widely varying lithology in overlapping core segments, the peat-mud contacts in Russian core R24 at the east edge of Botts Marsh (**Figures 5**, S1, S2, and S3) are too disturbed to infer paleoenvironmental change across them, and so we did not sample core R24 for microfossils.

All 95 samples of foraminifera (**Figures 7** and S4; Table S1) were refrigerated, prepared, and counted using standard methods (e.g., Scott and Hermelin 1993; de Rijk 1995; Kemp et al. 2009; Engelhart et al. 2013b; Milker et al. 2015a). Ten species of foraminifera were identified using the taxonomic illustrations and descriptions in Horton

and Edwards (2006), Hawkes et al. (2010), Wright, Edwards & van de Plassche (2011), and Milker et al. (2015a).

To make our transfer function reconstructions of RSL change across contacts consistent those of Kemp et al. (2018), we followed their procedures. We standardize our taxonomy, which differs slightly from the taxonomy for contact A of Hawkes et al. (2011; Table S1) by renaming *Trochamminita irregualris* to *Trochamminita* spp., and combining all species (*maniliensis* and *wilberti*) of *Haplophragmoides* and calcareous species into single groups, respectively. Similarly, we express foraminiferal assemblages as counts (Table S1) and exclude samples with <30 foraminifera from the reconstructions (e.g., Hawkes et al. 2011 and Kemp et al. 2018). Such low abundance assemblages may not be *in situ*, or may have undergone significant taphonomic change, and thus are likely unrepresentative of the environment at the time they were deposited. To check that our sample assemblages have good modern analogs in the Kemp et al. (2018) dataset, we used the same modern analog evaluation technique: all but one of our fossil samples containing >30 foraminifera (at 186 cm depth in core R5, Table S1) met a 10% dissimilarity threshold in pair-wise comparisons. Using "SWLI," a standard water level index that allows comparison among sites with differing tidal ranges (e.g., Horton and Edwards 2006; Kemp and Telford 2015), we equate mean higher high water (MHHW) with 200 SWLI and mean tide level (MTL) with 100 SWLI. At Nehalem these tide levels are 1.26 m (2.38 m NAVD88) and 0.01 m MTL (1.18 m NAVD88), respectively.

A key aspect of our application of a Bayesian transfer function to Nehalem foraminiferal assemblages is that we include prior information about sample lithology (Cahill et al. 2016) (**Figures 7** and S4; Table S1). Clastic dominated samples typical of tidal flats or low marshes are assumed to have accumulated between local mean low water (18.1 SWLI or −1.02 m MTL) and MHHW (200 SWLI or 1.26 m MTL). Alternatively, organic-rich sediment, which commonly reflects middle and high tidal marsh settings, is assumed to have accreted above local mean high water (182 SWLI or 1.03 m MTL); the upper bound of the latter is the highest occurrence of foraminifera in the Kemp et al. (2018) dataset (252 SWLI). Inclusion of the two stratigraphic priors does not set a limit on the elevations reconstructed by the Bayesian transfer function, but it does increase the probability that the elevations will fall within the specified range of the assigned stratigraphic prior. These stratigraphic priors overlap and are conservative, in that they allow the function to reconstruct RSL changes reflecting either submergence or emergence (Kemp et al. 2018).

Diatom analysis

To learn more about the scale and rate of changes in tidal environments in core V1, we also sampled three-quarters of its tidal sediment for diatoms at 1- to 3-cm intervals (0.33–2.88 m depths on **Figure 8**; sampling depths in the compacted vibracore were 0.31–2.60 m; Tables S2 and S3). The 160, 4- to 7-mm-thick, sediment samples were prepared using standard methods (e.g., Sawai, Nasu & Yasuda 2002; Sawai and Nagumo 2003). At least 300 diatom valves were identified in each sample under an oil-immersion microscope at 600x magnification. Fragments containing more than half a valve were included in the counts. We identified 314 species and forms in 76 genera in core V1 (Table S2). We show diatom abundance as a percentage of the total number of diatom valves counted, with only species that exceeded 5% of valves in more than five samples used for paleoecological interpretation (**Figure 8**, Table S3; e.g., Horton et al. 2007).

Although data on modern tidal diatom floras along Cascadia's coasts are available (Sawai et al. 2016a, 2016b; Hong 2019), a well-tested diatom transfer function, comparable to the Bayesian foraminiferal transfer function of Kemp et al. (2018), has not been published. The many hundreds of diatom species that make up the diverse assemblages typical of Cascadia tidal sequences have so far limited the degree to which modern diatom assemblages can be used as good analogs for fossil assemblages (e.g., Nelson et al. 2008; Hong 2019). For this reason, we use only abundance (percentage) data for the most common diatom species to qualitatively assess paleoenvironmental change across contacts in core V1 at the East Bank outcrop (**Figure 8**, Table S3).

Results—Stratigraphy, Ages, and Amounts of Coseismic Subsidence Across Earthquake Contacts

Nehalem River floodplain stratigraphy

Grant (1989), Minor and Grant (1996, their **Figure 3**), and Grant (unpublished 1994 report in Supplementary Files) studied an outcrop in a natural levee showing four buried soil A horizons with sharp upper peat-mud contacts on the north side of the Nehalem River 0.8 km upstream from its confluence with the North Fork Nehalem River (location 16 on **Figure 2**). Grant (unpublished 1994 report in Supplementary Files, "upstream" site of her **Figure 6**, her **Table 1**) mapped stratigraphy and plant fossils along 22 m of the outcrop, and determined the approximate times that the contacts of the buried A horizons formed with 12 ^{14}C ages on spruce stumps, peat, rooted herb rhizomes, and detrital materials, such as sticks and cones. The uppermost buried A horizon consists of a thin peaty silty mud containing abundant twigs and large rooted stumps of Sitka spruce sharply overlain by sandy silt. The second A horizon is a muddy peat with sticks and cones sharply overlain by sandy silt containing rhizomes of *Triglochin maritima*. The third A horizon is a faint, organic-rich mud overlain by wood fragments and silt. The lowest, fourth A horizon is a woody peaty mud, with large spruce stumps rooted in it, sharply overlain by a thin bed of fine sand. In 2006, we identified the younger three contacts at the tops of the four buried A horizons in the outcrop, and in 2009 the younger two contacts in cores 5 m inland from the outcrop. We could not find the lowest buried A horizon reported from the outcrop because too much silty mud had aggraded against the lower 60% of the original 1991 outcrop. By 2009, a winter storm had toppled four tall spruce trees into the river, preventing access to the outcrop.

Based on the sharpness of the upper contacts of the four A horizons, the amount of submergence indicated by upward changes in lithology and plant fossils across the contacts, and the similarity of the A horizon ages to ages for similar stratigraphic evidence of great earthquakes elsewhere at Cascadia (e.g., Atwater 1987, 1992; Atwater, Stuiver & Yamaguchi 1991; Nelson 1992a; Clarke and Carver 1992), Grant (unpublished 1994 report in Supplementary Files) and Grant and Minor (1996) concluded that at least the uppermost and lowermost contacts marked enough subsidence during great Cascadia earthquakes to lower spruce forests to the level of tidal flats. Our analysis of Grant's radiocarbon ages (unpublished 1994 report in Supplementary Files, her **Table 1**) from location 16 (**Figure 2**; methods described below), gave an age interval of 491–248 cal a BP for the uppermost sharp contact, 1108–751 cal a BP for the second sharp contact, 1550–1181 cal a BP for the third contact, and 1680–1389 cal a BP for the lowest sharp contact.

Our reconnaissance of outcrops elsewhere along the Nehalem River and the North Fork Nehalem River suggests that the floodplain of the lower valley records primarily fluvial sedimentation rather than tidal wetland sedimentation that would more clearly record the coseismic subsidence inferred by Grant (unpublished 1994 report in Supplementary Files) at location 16 (**Figure 2**). River outcrops 1- to 3-m-high south of the confluence of the rivers showed 1 to 2 m of fluvial silty mud and silty sand, occasionally overlying lesser thicknesses of silty tidal mud. In outcrops at locations 7, 11, 13, 14, and 15 the stumps of large spruce trees are eroding out of the river bank at about the same depth as a discontinuous, dark brown, decomposed A horizon, likely correlative with the youngest A horizon mapped by Grant (unpublished 1994 report in Supplementary Files) at location 16. The ~1-m depth of the horizon, which is comparable to depths of peat-mud contacts that we infer to mark wetlands suddenly submerged during the 1700 CE earthquake near the mouth of the river (below), suggests that trees rooted in the A horizons may have been rapidly buried about that time. Stumps overlain by fluvial silt and sand 1–2 m lower than the higher stumps at sites 7, 12, 13, and 14 also appear to be rooted in the dark brown, discontinuous remains of thin A horizons, probably recording an earlier rapid change in floodplain sedimentation that buried the trees and was, perhaps, correlative with the lowest rooted stumps dated by Grant (unpublished 1994 report in Supplementary Files; Losey 2002). However, because evidence of sudden land-level change in such largely fluvial sediment sections is difficult to distinguish from rapid sediment aggradation caused by river floods, fires, landslides, or other changes in the drainage basin (e.g., Kelsey et al. 1998), we did not investigate the floodplain outcrops further.

The stratigraphy beneath unforested lowland in the southern part of the Nehalem River valley (**Figures 2** and **3**) poorly preserves easily identifiable records of sudden land-level changes. Riverbank exposures, <1-m-high roadcuts, and floodplain elevations suggest that silty sediment within 2 m of the surface was either derived from valley side slopes or deposited in a freshwater fluvial environment. Eleven gouge cores at the two lowest sites east of the Nehalem River and northwest of Gallagher Slough exposed fluvial silty mud to silty sand in the upper 1.5 to 2 m (locations 8 and 9 on **Figure 2; Figure 3**). Estuarine clayey silt with fragments of bivalve shells beneath the fluvial sediment in two cores shows the minimum upstream extent of subtidal sediment, probably of pre-late Holocene age. Thin beds of dark, organic-rich mud in two other cores were too discontinuous to map laterally; no beds of wetland peat were found.

Nehalem Bay wetland stratigraphy

Grant and McLaren (1987), Grant (1989), and Grant (unpublished 1994 report in Supplementary Files) sought to determine the lateral extent of peat-mud contacts (mapped by them at the tops of buried A or O horizons) potentially marking earthquake subsidence through reconnaissance gouge coring in present-day marshes southwest, west, and northwest of the East Bank outcrop (**Figures 2** and **3**). In more than half their cores and examined outcrops along transects across Lazarus and West islands (the latter informally named), and 90% of their cores in Dean marsh, these authors found beds of peaty mud to muddy or sandy peat (at depths of 50–140 cm), sharply capped by coarse silt, sandy silt, silty fine sand, or fine sand. Much of the marshland west of Grant and McLaren's (1987) transects has developed since 1875 (Gilbert 1875; Johannessen 1961; Losey 2002: 422; Molino et al. 2016). North of Dean marsh in the area labeled Elk pasture (**Figure 3**), we examined 14 gouge cores along two perpendicular transects that showed tidal mud sharply to abruptly overlying high marsh peat at 50–60 cm depth. If, as we infer, all contacts correlate with contact A at the East Bank outcrop, the contact can be mapped at least 1.1 km west and 2 km northwest of the outcrop. Peaty beds whose upper contacts might be correlated with contacts B and C in the East Bank outcrop were found in only 6 of these 99 cores.

Grant and McLaren (1987) described about 2–50 cm of fine sand overlying contact A in about a third of the cores on Lazarus and West islands, and 1–4 cm of fine sand on the contact in half the cores near the northeastern edge of Dean marsh (**Figure 3**). Like Grant (1989), we infer all contacts to mark subsidence during the earthquake of 1700 CE followed by sand deposition by its tsunami. Grant's unpublished graphical core descriptions, however, are not sufficiently detailed or sand bed thicknesses sufficiently consistent for us to map the extent of sand deposition across wetlands in 1700 CE. Some >15-cm-thick sand beds in cores near river channels may be fluvial (e.g., Woodward, White & Cummings 1990).

Stratigraphy exposed at archeological sites and in gouge cores on the west side of Nehalem Bay suggests that shorelines subsided and were inundated by tsunamis as a result of the great earthquake of 1700 CE. Grant (1989) described five gouge cores near Cronin Point with 5–10 cm of woody to sandy peat sharply overlain by 20–30 cm of fine-to-medium sand (locations 1–3, **Figure 2**). About the same time, archeologists (Scheans et al. 1990; Woodward, White & Cummings 1990) interpreted stratigraphy at archeological sites near locations 1–4 (**Figure 2**) as the result of rapid estuarine habitat changes in the

past 400 years, caused either by migration in the positions of the Nehalem River channel or the Nehalem spit and dunes, or by subsidence and tsunami deposition in 1700 CE (Losey, Erlandson & Moss 2000). In far more thorough and better documented excavations of sites near Cronin Point, directed at understanding how people living on the shores of Nehalem Bay responded to the earthquake and tsunami of 1700 CE (e.g., Losey et al. 2005), Losey et al. (2000) and Losey (2002) concluded that cultural materials described by Scheans et al. (1990) and Woodward, White & Cummings (1990) near Cronin Point were reworked, perhaps but not necessarily due to erosion induced by earthquake subsidence. Losey's (2002) detailed excavations at each of three sites revealed organic-rich beds sharply overlain by sandy beds consistent with earthquake subsidence of shoreline soils and tsunami deposition. Stratigraphy, artifacts, and ages record occupation of two of the sites shortly after 1700 CE. In excavations southwest of location 1 (**Figure 3**), Minor et al. (1991) and Moss and Erlandson (1995) found evidence of occupation prior to 1700 CE but no conclusive evidence of earthquake subsidence or tsunamis. Farther northeast in an excavation about 100 m east of location 4 (**Figure 2**), Woodward, White & Cummings (1990) concluded that ceramic fragments, arrow points, and other cultural materials in a wetland peat had been buried by tsunami-deposited sand following sudden subsidence, although as Losey et al. (2000) point out, such materials may be reworked. Based on the sharply buried sandy peat at 60–90 cm depth in four 2009 cores at location 4, we concur that marshes along the northwest shore of the bay may have subsided suddenly in 1700 CE and were probably buried by sand deposited by a tsunami. These sites are 3.5 km west of the East Bank outcrop and 7 km southwest of the upstream outcrop described by Minor and Grant (1996; **Figure 2**, location 16).

East Bank outcrop – stratigraphy, ages, and earthquake subsidence

Contact A – Lithology and age

In her mapping of the sharp peat-mud contacts (by tracing four buried peaty soil O horizons) in the East Bank outcrop along the river, Grant (unpublished 1994 report in Supplementary Files) described the uppermost O horizon beneath contact A as varying from a slightly peaty mud to a fibrous peat containing forest litter and spruce cones overlain by mud to sandy silt hosting abundant growth-position rhizomes of *Triglochin maritima*. Our vibracores showed muddy peat to peat abruptly (contact <1 mm thick) overlain by peaty mud to coarse silt, with *T. maritima* 0.2–0.4 m above the contact (**Figures 4, 5**, S1, and S2). Spruce stumps and root systems several meters across mark the horizon along much of the outcrop.

Unusually precise ages for contact A are consistent with it forming through coastal subsidence during the great earthquake of 1700 CE (Nelson et al. 1995; Satake, Wang & Atwater 2003; Atwater et al. 2004). Nelson et al. (1995) dated the leaf bases and stems of the high marsh herbs, *Potentilla pacifica* and *Juncus* cf. *arcticus*, at contact A sticking up into overlying sandy silt. Rings cut from the outer parts of roots of *Picea stitchensis* and cf. *Pyrus fusca* rooted in the O horizon beneath contact A gave the most precise age for the contact and subsequent tree death of 269–15 cal a BP (1681–1935 CE). A fragment of a Native American utility basket, woven from *Chamaecyparis* or *Thuja* sp. bark and perhaps in use at the time of the earthquake (Connolly and Byram 1997; Atwater et al. 2005 p. 21), in mud at the contact is about the same age. Grant's (unpublished 1994 report in Supplementary Files, her **Table 1**) less precise ages on various materials above and below contact A are also consistent with coseismic subsidence in 1700 CE (**Table 1**). Even the two most precise ages for plant death about the time of contact A (128 ± 9 ^{14}C a BP and 179 ± 15 ^{14}C a BP, **Table 1**) have broad time ranges due to the pronounced plateau in the radiocarbon calibration curve during this period (**Figure 6**).

Contact A – Subsidence measured with foraminifera

We analyzed 22 samples in core V1 across contact A (between 1.09 to 1.32 m depth) for foraminifera (Table S1). This interval included a red-brown (7.5YR Munsell color hue) slightly muddy peat with in-place roots and wood fragments (1.32–1.22 m depth) sharply (≤3 mm) overlain by a slightly peaty mud with some roots and detrital plant fragments (1.22–1.09 m depth; **Figures 7A** and S1). In the slightly muddy peat below contact A, *Haplophragmoides manilaensis* (27–63%), *Balticammina pseudomacrescens* (5–43%) and *Trochammina irregularis* (9–17%) dominate the assemblage, reflective of a high to middle marsh environment (e.g., Hawkes et al. 2010; Engelhart et al. 2013a; Milker et al. 2015b). Above contact A, the assemblage is dominated by *Milliammina fusca* (0–61%) and *Jadammina macrescens* (0–100%), but few (<23) foraminifera per sample were found in the first 9 samples above the contact. Low numbers of these species (<30 tests/ml) are consistent with high deposition rates in a tidal flat or low marsh environment (Hawkes et al. 2010), or with slow rates of recolonization of foraminifera following subsidence (e.g., Horton et al. 2017).

Using an analysis of the posterior samples for SWLI values (provided by the Bayesian transfer function) for assemblages with >30 foraminifera above and below contacts (e.g., Figure S5), Kemp et al. (2018) reconstructed 1.1 ± 0.5 m of sudden RSL rise across contact A (**Figure 7A**). Submergence of 1.1 m is consistent with the changes in the foraminiferal assemblages and lithological changes across the contact. We infer that a suddenly flooded middle to high tidal marsh changed to a tidal flat. Hawkes et al (2011) used the same foraminiferal data to estimate 0.5 ± 0.3 m of coseismic subsidence across contact A, but that reconstruction used a previous non-Bayesian transfer function and was hampered by seven no-modern-analog fossil assemblages (no modern sample in the Hawkes et al. 2010, database was a good analog for the fossil assemblages) above the contact.

Contact A – Changes in diatom assemblages

The significant change in diatom assemblages across contact A (sampled every 10 mm from 0.22 m above contact A to 0.18 m below it) is consistent with the change in lithology across contact A and with the changes in tidal environments inferred from the foraminiferal

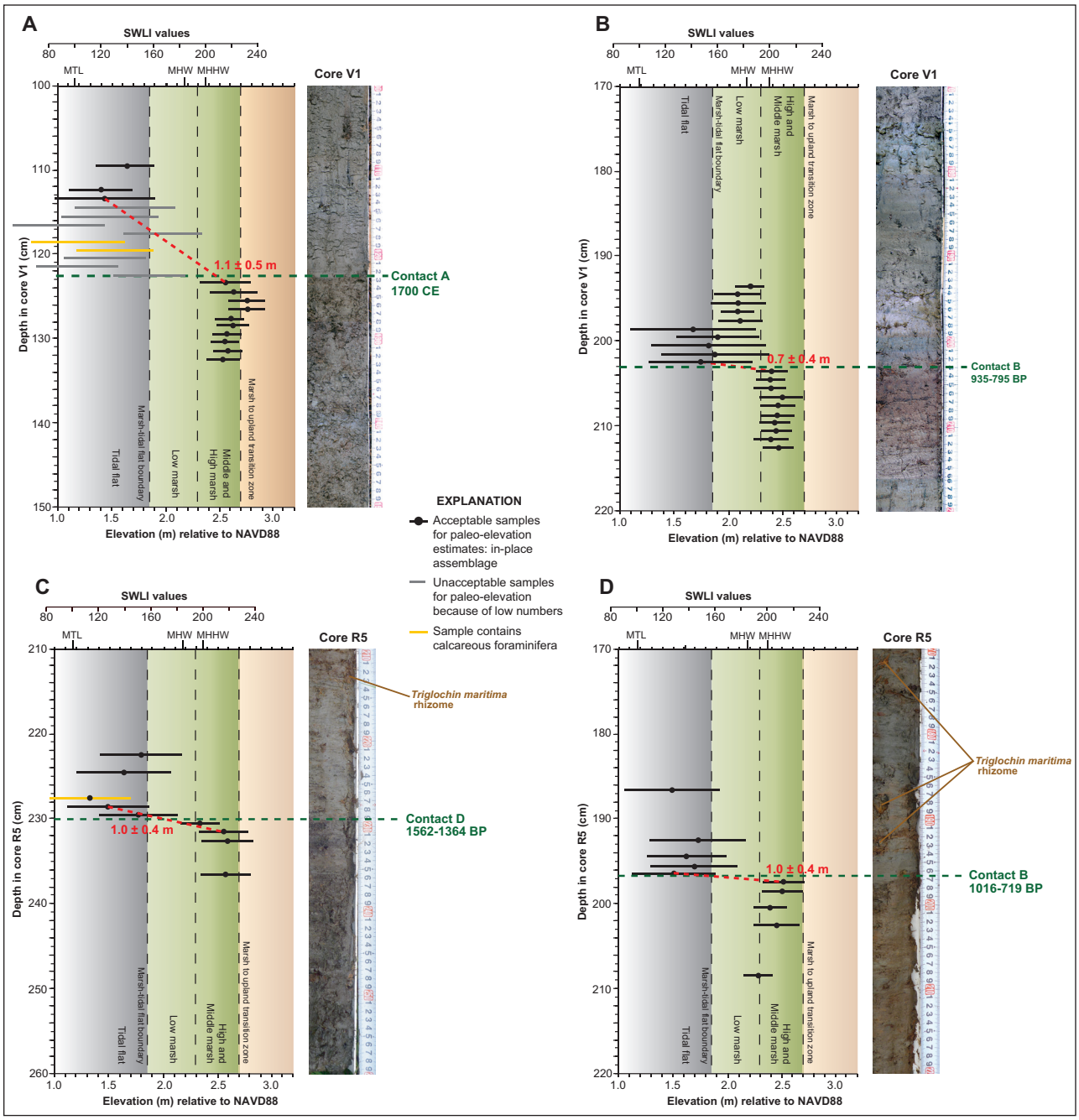

Figure 7: Reconstructed elevation (relative to NAVD88) near contacts A, B, and D in vibracore V1 at the East Bank outcrop (Figures 3 and 4) and Russian core R5 from Botts marsh (Figure 5) using the Bayesian foraminiferal transfer function of Kemp et al. (2018) with fossil assemblages (data in Table S1). To compare our subsidence reconstructions with the results of previous foraminiferal transfer function reconstructions elsewhere, we show reconstructed subsidence with ±1σ errors. Approximate gradational boundaries between elevational zones based on vascular plant communities observed by Eilers (1976) on West Island, Hawkes et al. (2010) west of Dean marsh, by Laura Brophy and others (written communication, 2018) on West and Lazarus islands, and by us in Botts marsh (e.g., Janousek-Folger et al. 2014). SWLI values follow Kemp et al. (2018). Gray bars mark the depths of analyzed samples with too few foraminifera to be meaningful in reconstructing elevation (Table S1). Red numerals indicate the amount of subsidence (with Bayesian transfer function errors) across contacts (Table S1). Photographs to the right show sections of core: **(A)** contact A, 100–150 cm depth in core V1; **(B)** contact B, 170–220 cm depth in core V1; **(C)** contact D, 210–260 cm depth in core R5; **(D)** contact B, 170–220 cm depth in core R5. In (C) and (D), *Triglochin maritima* rhizomes in growth position in tidal flat mud are labeled above contacts D and B.

transfer function reconstruction (**Figures 7A** and **8**; Tables S2 and S3). Freshwater taxa, such as *Pinnularia*, or species with a fresh-to-brackish salinity preference, such as *Cosmioneis pusilla* and *Pinnularia lagerstedtii*, and brackish species, such as *Nitzschia pura* and *Navicula cinta*, dominate assemblages of the muddy peat beneath the contact. Although other species dominate the upper edge of a modern diatom transect on the north shore of

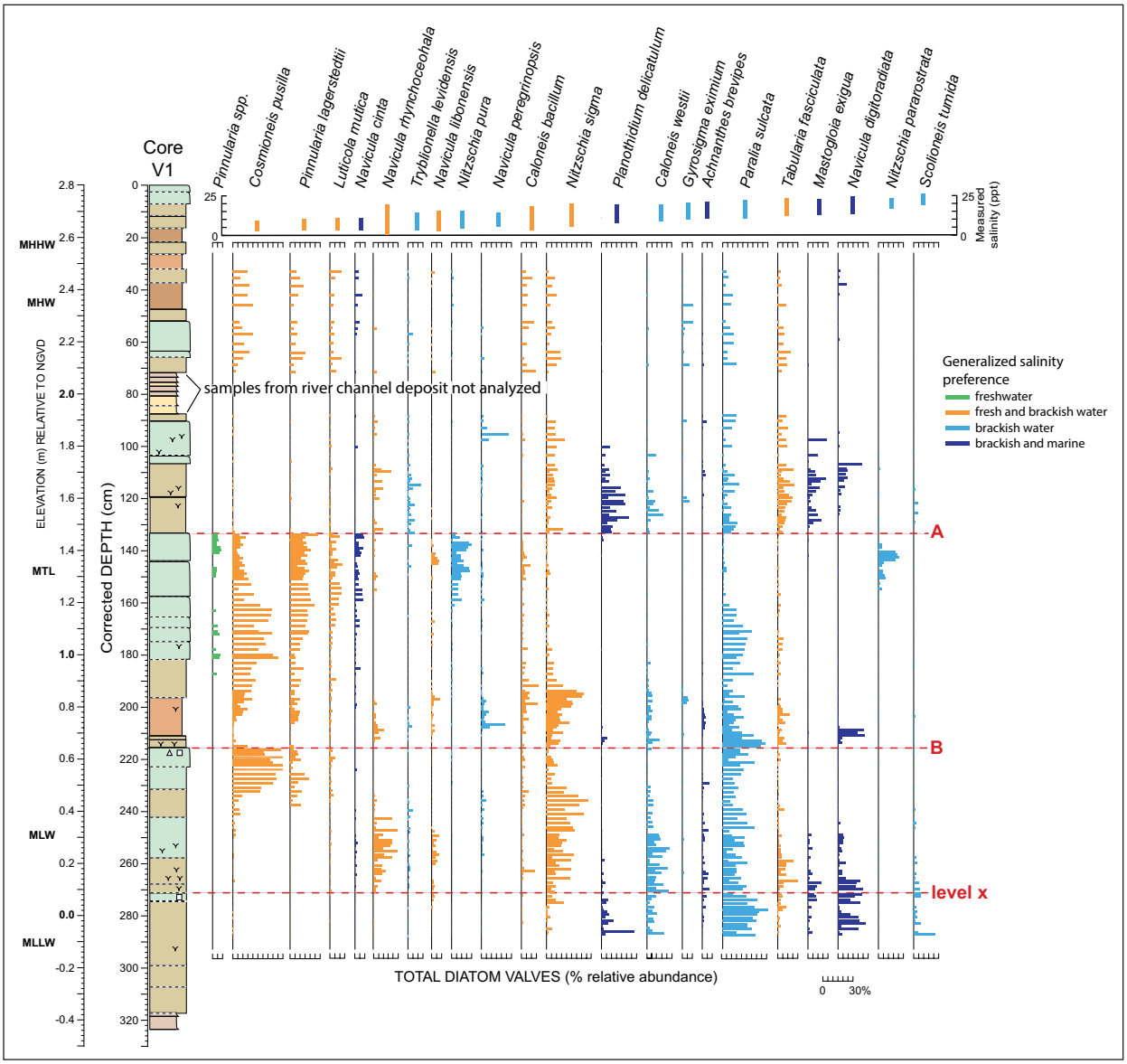

Figure 8: Relative abundance (percent of total valves counted) of diatoms in core V1. Species (those >5% in at least 5 of 160 samples) are listed in order of typical preferred salinity (ppt) range as measured for modern Oregon samples by Sawai et al. (2016a, their Table A2; Table S3). Colors highlight the general salinity preference of species. Depths and elevations for core lithologies on the left edge of the figure are uncompacted depths (which match those shown on Figures 5, S1, S2, and S3), as estimated from contact depths in adjacent gouge cores. On this figure, we adjusted the original sampling depths of the 160 samples to match their position relative to the uncompacted depths of contacts and units in the core. Depths of diatom samples shown on this figure do not match the original sampling depths on Table S3.

Nehalem Bay, such floras are typical of middle to high marshes in Oregon (Sawai et al. 2016a). Above the contact these species are absent in the peaty mud, which is dominated by largely brackish to brackish-marine species, such as *Planothidium delicatulum*, *Mastogloia exigua, Tabularia fasciculata*, *Achnanthes brevipes*, and *Nitzschis sigma*. In particular, *Planothidium delicatulum* and *Mastogloia exigua* prefer brackish environments, as found mainly on muddy tidal flats (Sawai et al. 2016a). *Paralia sulcata* is also a common species in our samples, but may be transported (e.g., Hemphill-Haley 1995; Sawai 2001; Sawai, Nasu & Yasuda 2002; Dura et al. 2016b).

Contact B – Lithology and age

Contact B, between muddy peat overlain by peaty mud to fine sand ~1 m below contact A, is abrupt and irregular along much of the outcrop as well as in the vibracores (**Figures 4, 5**, S1, and S2). *T. maritima* rhizomes are common just above the contact (Grant, unpublished 1994 report in Supplementary Files) and a few were found in the vibracores. A minimum age on growth-position *T. maritima* rhizomes 2 cm above contact B in the outcrop, and an averaged age on a woody herb rhizome at contact B (which may be detrital) and fragments of wood and needles in the muddy peat below the contact in the vibracores, gave an OxCal-modeled

age interval for contact B of 942–764 cal a BP (**Table 1; Figure 6**).

Contact B – Subsidence measured with foraminifera

We analyzed 20 samples in core V1 across contact B (between 1.93 to 2.12 m depth; Table S1). This interval included a muddy peat, sharply overlain by a peaty mud with roots and *Triglochin maritima* rhizomes and plant fragments (**Figures 5** and **7B**). In the muddy peat below contact B, the foraminiferal assemblage is dominated by *B. pseudomacrescens* (7–59%), *J. macrescens* (26–81%), and *T. inflata* (2–16%), reflecting a high to middle marsh environment. Above contact B, the assemblage is dominated by *J. macrescens* (23–68%), *M. fusca* (2–41%), *T. inflata* (0–54%) and *B. pseudomacrescens* (5–19%), typical of Oregon low and middle marshes (e.g., Hawkes et al. 2010; Engelhart et al. 2013a; Milker et al. 2015a).

Based on consistent Bayesian transfer function reconstructions of elevation for samples above and below contact B, we reconstruct 0.7 ± 0.4 m of submergence across the contact (**Figure 7B**; Table S1). The reconstructed elevations suggest that a middle to high marsh suddenly changed to the highest environments of a tidal flat or the lowest parts of a low marsh and then gradually shoaled to a higher low marsh.

Contact B – Changes in diatom assemblages

Changes in diatom assemblages across contact B (sampled every 10 mm from 0.22 m above the contact to 0.57 m below it) are consistent with the submergence reconstructed with the foraminiferal transfer function (**Figures 7B** and **8**; Tables S2 and S3). As in the muddy peat beneath contact A, the fresh-to-brackish species *Cosmioneis pusilla* and *Pinnularia lagerstedtii* are common below contact B, although no freshwater species are present. *Paralia sulcata* is also a dominant species, but may be transported. The brackish-marine species *Navicula digitoradiata* and *Planothidiumm delicatulum* make an appearance above the contact whereas *Nitzschia sigma*, a species common in fresh-brackish water, slowly increases above the contact. Such changes in floras suggest less subsidence across contact B than across contact A, perhaps from a higher middle marsh or low high marsh to a tidal flat or low marsh.

Contact C and level x – Lithology and age

Grant (unpublished 1994 report in Supplementary Files) reported that peat-mud contact C, at the top of the third buried O horizon, was similar to contact B. In contrast, where we found it, 0.2–0.5 m below the base of the 2009 outcrop, an indistinct contact C separated slightly peaty mud from overlying silty mud with abundant *T. maritima* rhizomes. The single minimum age for contact C from the face of the outcrop, on *T. maritima* rhizomes 2 cm above the contact, gives a calibrated age of 1119–915 cal a BP (**Table 1; Figure 6**).

We could not confidently identify contact C in any of the four the vibracores taken 3–4 m east of the face of the outcrop (**Figure 4**). Extremely faint color and textural changes in peaty mud 0.1–0.2 m below some *T. maritima* rhizomes in core V1 (note minimal changes in Troels-Smith lithologies on Figures S1 and S3 at ~2.43 cm depth; Figure S4A) are too indistinct and gradational to identify as a contact correlative with contact C, and no lithologic changes at this depth could be identified in the other vibracores. For this reason, we refer to this depth in the vibracores only as "level x." An OxCal-modeled age interval for level x using four almost identical (two maximum and two minimum) ages from the equivalent depth in vibracores V3 and V4 shows that it is about the same age as contact C in the outcrop, or perhaps a century older (1180–1065 cal a BP; **Table 1; Figure 6**).

Contact C and level x – Changes in foraminiferal assemblages

In an effort to identify a rapid rise in RSL in core V1 that might correlate with contact C, we analyzed 17 foraminiferal samples near level x (between 2.25–2.60 m depth, Figure S4A). In the three lowest samples containing >30 foraminifera, the foraminiferal assemblage is dominated by *M. fusca* (50–100%), *J. macrescens* (0–20%), *T. inflata* (0–18%) and, *Haplophragmoides* spp. (0–10%), species typical of tidal flat to middle marsh environments (Table S1). In the nine higher samples, *J. macrescens* (0–80%), *M. fusca* (0–78%), and *T. inflata* (0–13%) dominate, as commonly found in tidal flat to low marsh faunas. Although the concentration of foraminifera in the sample nearest level x is high (213 tests/ml), concentrations of higher (27–112 tests/ml) and lower (21–88 tests/ml) samples are quite variable.

RSL elevations reconstructed with the Bayesian transfer function near level x suggest greater changes in RSL than reflected by the very indistinct changes in lithology, calling into question their accuracy. Regardless of their cause, the reconstructed elevations are too variable and inconsistent for us to estimate a change in RSL near level x. For example, an increase in elevation of ~0.9 m from 2.41 to 2.37 m is followed by a decrease of ~1.1 m from 2.37 to 2.34 m despite no change in lithology (Figure S4A). An absence of foraminifera below 2.50 m may indicate riverine freshwater sediment below that depth, as indicated by the river-channel deposits less than 0.3 m lower in the core (discussed below; Figure S1). If so, the presence of *M. fusca* in the three lowest samples may record a transition from a fluvial to a brackish tidal environment. We do not think that post-depositional taphonomic changes destroyed foraminifera originally present below 2.5 m because assemblages in sediment of similar lithology higher in the core are well preserved.

Contact C and level x – Changes in diatom assemblages

Diatom assemblages, sampled every 10 mm (from 0.36 m below level x upward to contact B), also suggest minimal environmental change near level x (**Figure 8**, Tables S2 and S3). The brackish-marine species *Caloneis bacillum* gradually increases upward near level x, but the abundance of other dominant species is either similar near level x or their abundance changes gradually above it. Thus, the changes in diatom assemblages suggest a gradual change in salinity or tidal level superimposed on a gradual shoal-

ing of the core site from prior to the time of level x to the formation of contact B.

Contact D – Lithology and age

We were unable to identify contact D, at the top of the lowest buried O horizon in the East Bank outcrop described by Grant (unpublished 1994 report in Supplementary Files) in gouge cores as a woody muddy peat overlain by sandy silt, and mapped by her as indistinct and discontinuous (**Figure 4**). In the vibracores, the section >0.3 m below level x consists of interbedded muddy sand and sandy mud with a few beds of sand and mud, which we interpret as river channel and overbank deposits (Figures S1, S2, and S3). This interpretation is supported by two 1.2- to 1.3-ka ages on moss stems and deciduous leaf fragments from a distinctly bedded, detrital peat at the base of core V1 (**Table 1; Figure 5**). Most of the section below –0.35 m NAV88 in cores V1–V4 was deposited by the river or in adjacent quiet water prior to deposition of the tidal mud near level x.

However, the distinguishing characteristic of Grant's (unpublished 1994 report in Supplementary Files) lowest contact (D) marked by a buried O horizon was clusters of large spruce stumps on the sloping tidal flat below the outcrop. In two of tens of 2009 gouge cores near rooted stumps on the tidal flat at the same level as contact D and ~12 m west of the outcrop, we recovered parts of an eroded spruce-forest O horizon under two of the largest stump roots, confirming the presence of an eroded soil in which the stumps were probably rooted. Two ages on *Picea stitchensis* needles and a cone from the upper 0.2 m of the eroded O horizon match Grant's (unpublished 1994 report in Supplementary Files) youngest age for contact D from a nearby stump (**Table 1**). We use only the youngest of these maximum ages, which gives a broad OxCal-modeled age interval for contact D at the East Bank outcrop of 1681–1244 cal a BP (**Table 1; Figure 6**).

Botts marsh – stratigraphy, ages, and earthquake subsidence

To determine the lateral extent of the four peat-mud contacts in the East Bank outcrop to the east, we studied the stratigraphy of Botts marsh, a 270-m by 700-m wetland that hosts the only laterally extensive record of RSL changes over thousands of years that we mapped in the Nehalem River valley lowlands (**Figures 2** and **3**). Stratigraphic exploration of Botts marsh began with 9 gouge cores described by Grant and McLaren (1987), which we followed with 40 additional gouge cores and a series of overlapping Russian core segments (cores R5, R17, and R24). Using detailed field descriptions of 16 cores (e.g., methods of Nelson 2015) and reconnaissance descriptions of 36 others, we correlated lithologies and contacts among cores throughout the marsh and with the stratigraphy at the East Bank outcrop (**Figures 4, 5**, S1, and S3; locations on Figure S2).

We identified four peat-mud contacts (A, B, D, and E), bounded by lithologies suggesting rapid submergence of the marsh that we correlated over distances of 150 to 450 m. The most distinct contacts sharply (≤3 mm thick) mark the tops of mud-peat couplets of silty mud grading upward into clayey silt; rooted, organic-rich clayey silt; rooted peaty silt; silty peat; and peat. Similar couplets have been interpreted as evidence for repeated coastal subsidence during great Cascadia earthquakes at tens of sites along much of the subduction zone and elsewhere (e.g., Dura et al. 2016a; Milker et al. 2016; Shennan, Garrett & Barlow 2016). Other contacts, including possible correlatives of contact C in the East Bank outcrop, are so indistinct or extend over such limited distances that we could not confidently correlate them across Botts marsh (**Figures 5**, S1, and S3). These less distinct contacts are more gradual (5–20 mm thick) and separate stratigraphic units of very similar lithology (Figure S1) suggesting less than a few tens of centimeters of submergence. We dated contacts A, B, D, and E and two less distinct possible contacts using plant macrofossils from cores R5, R17, and R24.

Contact A – Lithology and age

Contact A is the most distinct and most widespread contact in Botts marsh. In >80% of cores, this contact is marked by brown (10YR color hue) muddy peat to red-brown (7.5YR to 5YR hues) peat sharply overlain by rooted mud to peaty mud at depths of 0.6–1.0 m (**Figures 5, 7**, S1, and S3). We identified contact A in all 52 cores in Botts marsh, some as much as 660 m apart, suggesting that the marsh at the time the contact formed was nearly as extensive as it is today. Our two maximum ages for contact A in Botts marsh are similar to those for contact A at the East Bank outcrop (**Table 1**). Using the youngest maximum age of 190 ± 25 ^{14}C a BP and our assumed historical limit of 1850 CE, the OxCal age model gives a broad distribution of 290–125 cal a BP that overlaps the even broader age distributions for plant death at contact A at the outcrop (**Table 1, Figure 6**). Because of its distinctness and continuity there is little doubt that this contact correlates with contact A in the East Bank outcrop and was formed through subsidence during the great earthquake of 1700 CE.

Contact B and level z – Lithology and age

Contact B is less distinct than contact A. It separates rooted mud or peaty mud from underlying muddy peat (**Figures 7B, 7C**, and S1), commonly with abundant fossils of growth-position *Triglochin maritima* below and sometime above it (**Figures 5** and S3). The contact is sharp (≤3 mm thick) in only half the cores that reached it, but the sharpness is accentuated by laminae of sandy silt a few millimeters thick in cores 13, R5, and 39. Beds of sand and silty sand 5–6 cm above the contact in cores 18, 110, 05, and 09 may record a related unusual surge of sand-laden water, perhaps a tsunami that shortly followed subsidence marked by the contact. We correlated contact B among 21 cores, mostly in the northwestern and northeastern parts of the marsh intermittently over a distance of as much as 540 m (**Figures 5**, S1, and S3). Our OxCal age interval (95% CI) for contact B (1017–707 cal a BP), based on detrital conifer fragments and a probable minimum age on growth-position *Triglochin maritima*

rhizomes just below the contact, broadly overlaps the age distribution for contact B in the outcrop (942–764 cal a BP; **Figure 6** and **Table 1**).

Because of the greater depth of contact B in core R5 relative to nearby cores (**Figures 5**, S1, and S3), we initially searched for the contact higher in the core. The gradual (over 10 mm) upward change from slightly muddy peat overlain by muddier peat at 148 cm depth, which we label "level z," is indistinct, but similar indistinct contacts of about the same age have been considered as evidence for subsidence during great Cascadia earthquakes (Atwater and Hemphill-Haley 1997; Milker et al. 2016). However, we were unable to confidently correlate level z to similar more distinct contacts in other cores, and two maximum-limiting ^{14}C ages near level z in core R5 show that this level is probably much younger (706–363 cal a BP, 95% CI) than contact B at the East Bank outcrop (942–764 cal a BP; **Table 1; Figure 6**). In a final test of the significance of level z as a possible earthquake contact, foraminiferal assemblages across it show no significant change in environment, consistent with its minimal change in lithology (Table S1; Figure S4C).

Contact B and level z – Subsidence measured with foraminifera

To help confirm our correlation of contact B in core R5 with contact B in core V1, we analyzed foraminiferal assemblages in five samples above and five below an abrupt (1-mm) contact at 1.97 m separating a red-brown, high-marsh peat with 7.5YR hues from a slightly peaty mud (**Figures 8D** and S1). The upper four of the five samples from the peat are dominated by *T. inflata* (13–43%), *J. macrescens* (25–34%), *Haplophragmoides* spp. (9–28%), and *B. pseudomacrescens* (4–32%), reflecting a middle to high marsh environment (Table S1). Above contact B, the assemblages are dominated by *J. macrescens* (25–39%), *M. fusca* (13–42%), *T. inflata* (12–31%), and *Ammobaculites* spp. (5–31%), taxa typically abundant in muddy tidal flats and low marshes. Lower foraminiferal concentrations above the contact (95–127 tests/ml, Table S1) than those below (127–167 tests/ml) may indicate slightly lower deposition rates above versus below the contact.

Bayesian transfer function reconstructions of elevation using the two samples immediately above and below contact B in core R5 show submergence across the contact of 1.0 ± 0.4 m (**Figure 8D**; Table S1). The reconstruction suggests that a middle to high marsh was suddenly changed to a tidal flat or lower low marsh.

Contact C – Lithology and age

Contact C, which is discontinuous but mappable along >210 m of the East Bank outcrop (**Figure 4**), was difficult to find in Botts marsh. Assuming our correlation of contact B across the marsh is accurate, we noted possible correlatives of contact C—sharp contacts with changes in lithology similar to those of contact B—in only 5 of the 31 cores that reached the next lower contact (D; Figure S3). Because none of the three cores that we sampled for radiocarbon include contact C, we have no OxCal age interval for it in Botts marsh.

Contact D – Lithology and age

Contact D is the second most lithologically distinct contact, and although reached in fewer cores throughout the marsh (31), it is sharp in a greater proportion of cores (>90%) than is contact A. Especially in cores in the central and eastern marsh, an abrupt (<1 mm) contact separates red-brown (7.5YR hue) high-marsh peat from overlying rooted mud or peaty mud (10YR to 2.5Y hues; **Figures 5, 7C**, S1, and S3). High salt marsh apparently extended over much of the northern and eastern part of the present-day marsh at the time contact D formed. An 18-mm-thick interval of peaty mud with traces of very fine sand above the contact in core R5 suggests an unusual surge of water at the time the contact formed. As in core V1 at the East Bank outcrop, we infer from its absence in cores that contact D has been eroded and replaced by younger river channel and overbank deposits in an area 50–100 m wide along the western edge of the marsh near the river (**Figures 5**, S1, S2, and S3).

The age of contact D in Botts marsh is bracketed by the youngest two of nine maximum ages on detrital materials in muddy peat below the contact, and by a minimum age on a leaf base of *Triglochin maritima* 1–3 cm above the contact. Using these maximum and minimum ages, the OxCal age model gives a 95% interval of 1568–1361 cal a BP for the contact in core R24 (**Table 1; Figure 6**). As this interval falls well within the broader modeled interval for contact D at the East Bank outcrop, we infer it to be the most accurate age for contact D and correlate this contact with contact D at the East Bank outcrop and the adjacent stumps on the tidal flat (**Table 1; Figures 4, 5**, S2, and S3).

Contact D – Subsidence measured with foraminifera

In core R5 five samples were taken above and four below 1-mm contact D at 2.30 m, which separates a high-marsh peat from a peaty mud to muddy peat above it (**Figures 7D** and S1). Assemblages in the four samples from the peat consist mostly of *Haplophragmoides* spp. (43–56%), *Trochamminita* spp. (9–18%), *B. pseudomacrescens* (9–26%), *J. macrescens* (5–15%), and *T. inflata* (3–11%), reflecting a high to middle marsh environment (Table S1). Above contact D, the assemblages are dominated by *M. fusca* (20–72%), *J. macrescens* (14–48%), and *Haplophragmoides* spp. (5–50%), similar to assemblages found in muddy tidal flats and low marshes in Oregon.

Bayesian transfer function reconstructions for the two samples immediately above and below contact D give elevations closer to each other than for upper and lower samples suggesting lesser or perhaps gradual submergence across the contact. But wood and a little sand in the sample above the contact suggest that it was deposited rapidly as a mixture of different materials, probably by a tsunami, and so its assemblage is unlikely to be representative of a stable tidal environment (e.g., Kemp et al. 2018). The sample below the contact consists of peat with minor amounts of wood. The 6% *M. fusca* and the presence of *Ammobaculites* spp. (1%;

Table S1), species typically found on tidal flats and in low marshes (Engelhart et al. 2013a; Milker et al. 2015a), in this sample is likely due to infiltration of foraminiferal tests from above the contact into cracks in the peat (e.g., Engelhart et al. 2013b; Milker et al. 2016; Kemp et al. 2018). Because assemblages in the two samples closest to the contact may not accurately reflect pre- and post-submergence environments, we infer that submergence across contact D was closer to the difference between the reconstructions for samples at 228.5 cm and 231.5 cm depths (1.0 ± 0.4 m) than between the difference for the samples closest to the contact (229.5 cm and 230.5 cm depths; 0.6 ± 0.4 m) (**Figure 7D**; Table S1). The greater difference (1.0 m ± 0.4 m) is more consistent with the lithologic changes across contact D in Botts marsh cores (**Figures 5**, S1, and S3) and with Grant's (unpublished 1994 report in Supplementary Files) description of contact D in the East Bank outcrop.

Contact E – Lithology and age

Contact E, stratigraphically below the contacts in the East Bank outcrop, was tentatively identified in 10 cores (R5, 9, 39, 11, R17, 03, 37, 35, 38, and 24) spanning a distance of 250 m along the upper edge of the northern and eastern marsh (**Figures 5**, S1, S2, and S3). Although the contact between muddy peat and overlying peaty mud is sharp in 5 of the cores, in 4 others (for example, in core R5, Figure S4) 1–3 cm of muddy peat alternates with 2–3 cm of mud and peaty mud in the interval 5–15 cm above the contact. Such alternating lithologies suggest fluctuating marsh environments rather than many decimeters of sudden tidal flooding. Using an average of three maximum ages on detrital materials in the muddy peat beneath contact E in cores R17 and R24, our Botts marsh OxCal model gives a maximum-age interval (95% CI) of 1857–1570 cal a BP for the contact (**Table 1; Figures 5** and **6**).

Contact E – Foraminiferal assemblages

Although the two samples from the muddy peat at 2.57–2.59 m contain assemblages typical of a middle to high marsh (largely *Haplophragmoides* spp., *J. macrescens*, *B. pseudomacrescens*, and *Trochamminita* spp.), none of the other 11 samples from core R5 contain sufficient numbers of foraminifera (>30) to make paleoenvironmental interpretations (Figures S1 and S4B, Table S1). Thus, no elevational reconstructions are possible for most of this segment of core R5. The lack of foraminifera suggests that, except for the two muddy peat samples, this section of core R5 may record largely freshwater environments.

Discussion—Earthquake Correlation, Timing, and Size

Like many before us (Atwater 1992; Nelson, Jennings & Kashima 1996; Atwater and Hemphill-Haley 1997; Kelsey et al. 2002; Nelson, Kelsey & Witter 2006; Milker et al. 2016), we use the degree of overlap among our modeled age distributions for Nehalem peat-mud contacts and the distributions for other sites as one of several criteria to assess whether or not the Nehalem contacts may record megathrust ruptures hundreds of kilometers long. Unlike the quantitative overlap comparisons of Hutchinson and Clague (2017), our comparisons (**Figure 9**) are only qualitative because the dating uncertainties for Nehalem contacts make quantitative comparisons with other sites uncertain. Another difference between our analyses and theirs is that Hutchinson and Clague (2017) pooled ages, mostly maximum ages, from the five central Cascadia sites whose age distributions they compared, whereas (as explained above) we selected the youngest, high-quality, maximum-limiting age, and in many cases an oldest minimum age (e.g., Goldfinger et al. 2012; Milker et al. 2016), to model the times of earthquakes or tsunamis at 13 sites between the Columbia River and Cape Blanco (**Figure 9**). In the selection process we evaluated available ages <2000 cal a BP from the 13 sites (235). About 137 of these are compiled by Leonard et al. (2010), Goldfinger et al. (2012), Engelhart et al. (2015), and Hutchinson and Clague (2017); another 98 ages, from Lewis and Clark River, Netarts Bay, Siletz Bay, Alsea Bay, and this paper, are unpublished.

Contact A – 1700 CE

Based on the <1.5-m depth of the distinct change in lithology across contact A, its cap of fine, well sorted sand in tens of cores on Lazarus and West islands, the distinct change in diatom assemblages, the foraminiferal transfer function reconstruction of 1.1 ± 0.5 m of subsidence across it, the >7-km distance over which its probable stratigraphic evidence in the lower Nehalem River valley extends (Minor and Grant 1996), and its age relative to the ages of similar evidence at similar depths at other sites (**Figures 2, 3, 4, 5, 6, 7A, 9**, S1, and S3; **Table 1**), we infer that contact A was produced by coseismic coastal subsidence and correlate it with similar evidence attributed to the 1700 CE earthquake and tsunami along much of the subduction zone (e.g., Nelson et al. 1995; Nelson, Kelsey & Witter 2006; Atwater and Hemphill-Haley 1997; Witter, Kelsey & Hemphill-Haley 2003; Atwater et al. 2004; Graehl et al. 2014; Valentine et al. 2012; Wang et al. 2013; Milker et al. 2016; Hutchinson and Clague 2017; Padgett 2019).

Our reconstructed submergence for contact A is consistent with subsidence during a great earthquake rupture (or several closely spaced ruptures) hundreds of kilometers long. Estimates of earthquake magnitude based on modeling the 1700 CE tsunami in Japan (Satake et al. 1996; Satake, Wang & Atwater 2003) suggest a long rupture as well. Subsidence marked by contact A is similar to the estimates for correlative contacts at Nestucca Bay (1.1 ± 0.5 m) and Salmon River (1.4 ± 0.4 m) (Kemp et al. 2018), 58 km and 75 km to the south, respectively (**Figures 1** and **9**). Hemphill-Haley's (1995; Atwater and Hemphill-Haley 1997) diatom-based estimate of >1.1 m at Willapa Bay, 100 km to the north, is also consistent with these estimates, as are the Bayesian foraminiferal values for the 1700 CE contact at Willapa Bay (1.3 ± 0.8 m) calculated by Kemp et al. (2018; data of Sabean 2004 as modified by Wang et al. 2013) and the semi-quantitative estimate using pollen and diatoms of 1.0 ± 0.5 m for the same contact at the Johns River, 134 km to the north (Shennan et al. 1996). However, Padgett's (2019) Bayesian foraminiferal

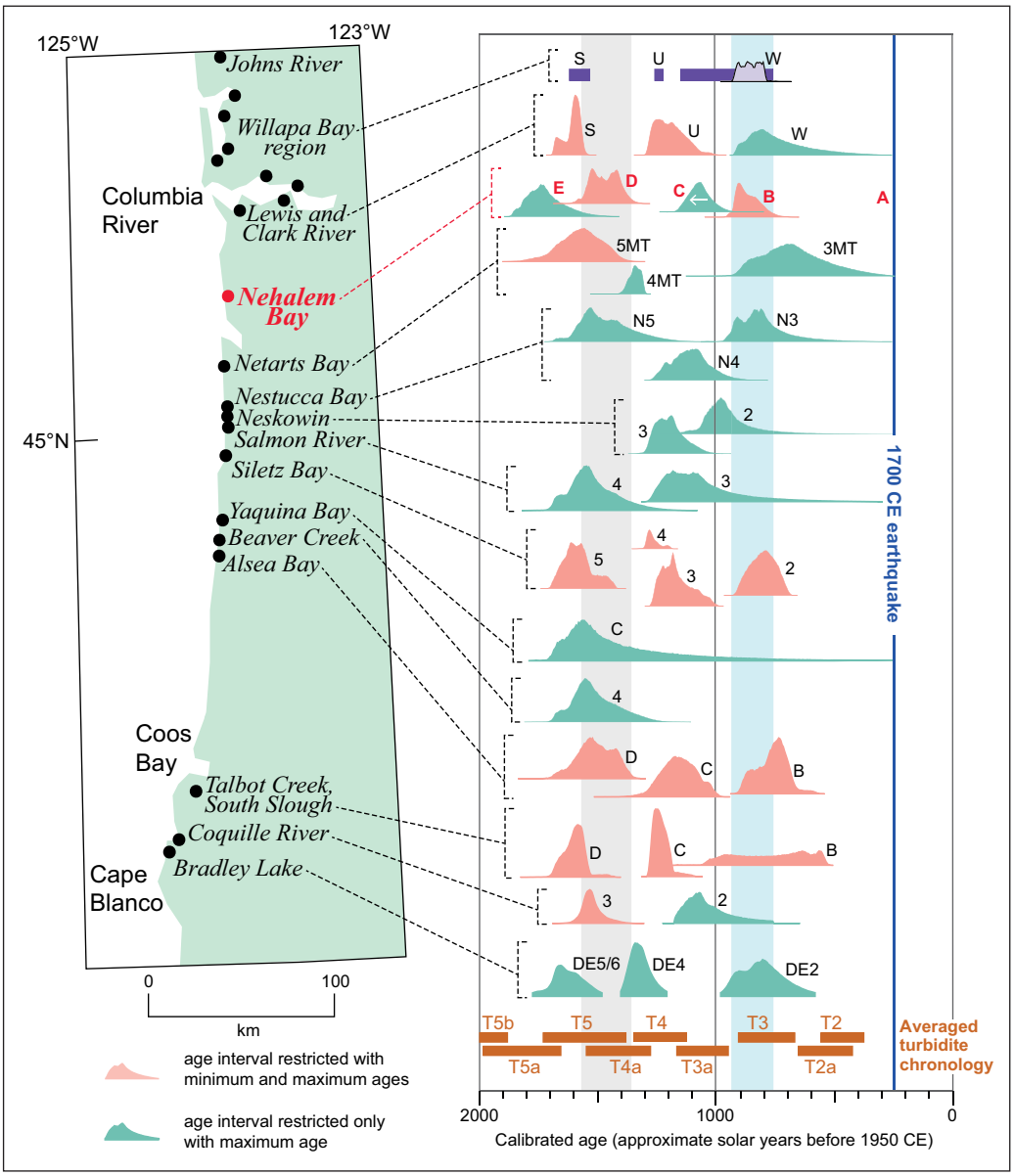

Figure 9: Radiocarbon-age probability distributions for evidence of great earthquakes and their accompanying tsunamis of the past 2000 years at 13 sites (dots on map at left) between the Columbia River and Cape Blanco. Distributions calculated from maximum-limiting (green) or minimum- and maximum-limiting (pink) ages with the sequence feature of OxCal (Bronk Ramsey 2008, 2009). Red labels mark distributions for contacts at the Nehalem River estuary. Ages used were selected from 235 published (Witter, Kelsey & Hemphill-Haley 2003; Witter et al. 2009, 2011, 2013; Kelsey et al. 2005; Nelson, Asquith & Grant 2004; Nelson, Kelsey & Witter 2006, 2008; Peterson et al. 2010; Graehl et al. 2014; Milker et al. 2016; Hutchinson and Clague 2017) and 106 unpublished ages. Shaded columns show the 95% CI range for distributions for contacts B and D (Figure 6). Age intervals (purple bars) for sites in the Willapa Bay region, mostly based on the ages of rings from stumps inferred to have died shortly after earthquake subsidence, are those of Atwater et al. (2004; Hagstrum, Atwater & Sherrod 2004). The probability distribution in front of interval W (light purple), is a more precise estimate calculated from the average of three ages reported by Atwater and Griggs (2012 p. 22). The three ages were also used in the age model for Lewis and Clark River. Age ranges for marine turbidites offshore are those of Goldfinger et al. (2012; averaged corrected ages, Appendix 1, Land-marine data tab).

estimates for subsidence in 1700 CE from four sites in Willapa Bay and Johns River are more variable (0.4 ± 0.4 m to 1.5 ± 0.5 m).

But subsidence at Nehalem in 1700 CE was much larger than that for its neighbor site at Netarts Bay only 35 km to the south (0.4 ± 0.3 m) (Shennan et al. 1998; Wang et al. 2013; Kemp et al. 2018) (**Figure 9**). To explain the change from 1.1 m to 0.4 m of subsidence over only 35 km Kemp et al. (2018) theorized that the smaller subsidence at Netarts was the result of greater along-strike differences in megathrust slip or rupture geometry than modeled by Wang et al. (2013), post-seismic uplift too rapid for foraminifera to recolonize to (e.g., Horton et al. 2017), or a combination of the two. Although Bayesian transfer function reconstruction errors are large, a 1:7 difference in modeled subsidence for the same earthquake over such a short distance suggests the assumption that the amount of coseismic subsidence at a coastal site is proportional to

rupture extent and earthquake magnitude may not apply for some earthquakes. Padgett (2019) discusses these and other potential reasons for the variability in his Bayesian transfer function estimates of subsidence during the 1700 CE earthquake in southwestern Washington.

Contact B – 942–764 cal a BP

Contact B, typically separating muddy peat from peaty mud or rooted mud, is considerably less widespread and distinct than contact A. We correlate it, however, 350 m east-west in Botts marsh and >210 m north-south along the East Bank outcrop. A few millimeters of silty fine sand near contact B in seven Botts Marsh cores suggest inundation of the marsh by a tsunami. Our OxCal age intervals for contact B at the East Bank outcrop (942–764 cal a BP) and in Botts marsh (1017–707 cal a BP) are consistent with the correlation of contact B with the top of the second youngest buried A horizon described by Grant (unpublished 1994 report in Supplementary Files) 5 km upriver at site 16 (**Figures 2, 3, 4, 5, 6**, S1; **Table 1**). The foraminiferal transfer function estimates of RSL rise across the contact of 0.7 ± 0.4 m in core V1 and 1.0 ± 0.4 m in core R5 differ by a third; the greater value in core R5 is probably due to the presence of *Ammobaculites* spp. in the samples just above the contact (Table S1) (e.g., Kemp et al. 2018). As the diatom assemblages in core V1 are consistent with a 1-m rise in RSL across contact B, we attribute the difference in subsidence between the two cores entirely to statistical variation (the 1σ errors of the two measurements substantially overlap). If coseismic as we infer, the 0.7–1.0 m rise in RSL is consistent with a great earthquake rupture hundreds of kilometers long.

The closest estimate of coseismic subsidence for a correlative of contact B is at Willapa Bay, 100 km north of Nehalem. Although based on a semi-quantitative index, Atwater and Hemphill-Haley's (1997) estimate of subsidence marked by the upper contact of their soil W, buried about the time of contact B (**Figure 9**), is <1 m, consistent with our Nehalem value.

The more precise of our OxCal age intervals for contact B (942–764 cal a BP, East Bank outcrop, **Figure 6**) overlaps substantially with OxCal distributions for 9 of the sites on **Figure 9** from Willapa Bay to southern Oregon, a distance of 400 km. The interval also overlaps with the age range for offshore turbidite T3, one of the thicker and more widespread turbidites of the marine record (Goldfinger et al. 2012). As a great earthquake rupture hundreds of kilometers long is consistent with 0.7–1.0 m of coseismic subsidence, contact B at Nehalem likely correlates with much previously published coastal evidence (e.g., Atwater et al. 2004; Kelsey et al. 2005; Nelson, Kelsey & Witter 2006, 2008; Schlichting and Peterson 2006; Witter et al. 2009; Milker et al. 2016; Minor and Peterson 2016; Hutchinson and Clague 2017) for a great earthquake about this time. But whether or not the subsidence at these sites was produced during one or several earthquake ruptures, and where the ruptures initiated, cannot be determined with our data from Nehalem. In their summary of evidence and ages for a great earthquake about this time, Hutchinson and Clague (2017) noted tsunami evidence for two discrete earthquakes, suggesting that contact B may record a great earthquake that did not rupture the entire subduction zone.

Contact C – 1119–915 cal a BP

Although Grant (unpublished 1994 report in Supplementary Files) mapped contact C for >210 m along the East Bank outcrop (**Figure 4**), we were unable to find it in the vibracores adjacent to the outcrop or correlate it more than a few tens of meters across Botts marsh (**Figures 5**, S1, S2, and S3). Neither foraminiferal nor diatom assemblages in core V1 at the stratigraphically equivalent depth (level x) of contact C in the outcrop show any significant change in tidal environments across the contact. Possible correlatives of contact C in the few Botts marsh cores where we found them are indistinct compared with contacts A and B. River deposits in the lower parts of some cores in the western part of the marsh suggest that a former contact C in these cores may have been eroded by a river channel to the east of the present channel (Figures S1, S2, and S3).

We infer that at the time contact C formed at the outcrop, the core-V1 site, and probably the sites of some of the other cores in the marsh with possible contact-C correlatives, were lower low marsh whose tidal flooding during possible coseismic subsidence recorded by contact C in the outcrop produced little change in lithology or microfossil assemblages. As illustrated by Nelson, Kelsey & Witter (2006, their **Figure 3B**), whether or not coseismic subsidence is recorded by distinct changes in tidal marsh litho- and bio-stratigraphy in a core depends on which tidal environments contemporaneous with the earthquake the core penetrates (e.g., Nelson 1992a; Nelson, Asquith & Grant 2004).

Although the broad, minimum-age, 95% CI probability distribution for the sample limiting the age of contact C at the East Bank outcrop (1119–915 cal a BP, **Figure 6**) significantly overlaps 7 of the sites of **Figure 9**, the distribution does not overlap the 95% CI age distribution for the burial of the third A horizon at the upstream site described by Grant (unpublished 1994 report in Supplementary Files) (1550–1181 cal a BP, location 16) or, notably, the precise interval for earthquake U at Willapa Bay (Atwater et al. 2004). Although Grant (unpublished 1994 report in Supplementary Files) inferred that contact C at the outcrop might record coseismic subsidence during a great earthquake, our inability to map the contact beyond the outcrop across Botts marsh precludes the argument that it records substantial subsidence during a great earthquake. Although a number of coastal sites host evidence for a great earthquake older than contact B and younger than contact D (e.g., those cited in Hutchinson and Clague 2017), we found no extensive evidence for such an earthquake in lowland areas of the Nehalem River estuary.

Contact D – 1568–1361 cal a BP

Based on the sharp (≤3 mm) contact at the top of bright-colored, 7.5YR-hue peat in many cores, high tidal marsh extended over much of the northern and eastern part of Botts marsh at the time that contact D recorded a rapid change to a tidal flat. Radiocarbon ages from cores R5, R17, and R24, as well as from tidal-flat stumps at the East

Bank outcrop, confirm that contact D is as widely distributed across Botts marsh as contact A (**Figures 4** and **5; Table 1**). Correlation to the fourth buried A horizon described by Grant (unpublished 1994 report in Supplementary Files) is suggested by three ^{14}C ages obtained by her from stumps rooted in the A horizon at site 16 (**Figure 2**). As for contacts A and C, our transfer function reconstruction of subsidence across contact D, 1.0 m ± 0.4 m, is consistent with a megathrust rupture along many hundreds of kilometers of the subduction zone.

No useful quantitative estimates of coseismic subsidence exist for contact-D equivalents at sites within 250 km of Nehalem. Semi-quantitative estimates are consistent with our Nehalem subsidence for contact D: Atwater and Hemphill-Haley's (1997) estimate of >1 m using diatoms across the upper contact of their soil S at Willapa Bay, and Shennan et al.'s (1996) estimate of 1.0 ± 0.5 m using pollen and diatoms at Johns River, 134 km north of Nehalem (**Figure 9**).

Our age distribution for contact D overlaps all age distributions for a probable correlative contact on **Figure 9** (Neskowin lacks a deposit in this age range and so is an exception). It also overlaps substantially with the age range for turbidite T5, one of the thickest and most extensive of the turbidites in the offshore sequence of Goldfinger et al. (2012). Our stratigraphic evidence at Nehalem and similar evidence from many of these other sites suggests that this contact marks a great earthquake that ruptured much of the subduction zone about 1568–1361 cal a BP (e.g., Atwater 1992; Nelson 1992a; Atwater and Hemphill-Haley 1997; Hutchinson et al. 2000; Kelsey et al. 2002; Witter, Kelsey & Hemphill-Haley 2003; Atwater et al. 2004; Nelson, Kelsey & Witter 2006; Peterson et al. 2010; Valentine et al. 2012; Graehl et al. 2014; Milker et al. 2016; Minor and Peterson 2016; Hutchinson and Clague 2017). Such evidence led Nelson, Shennan & Long (1996; and Nelson, Kelsey & Witter 2006), among others (e.g., Milker et al. 2016), to suggest that contact D records an earthquake as large or larger than the one in 1700 CE.

Contact E – 1857–1570 cal a BP

Contact E probably marks a rapid local change in tidal and freshwater environments, perhaps limited to Botts marsh, rather than a RSL change caused by regional subsidence during a great earthquake. We correlated contact E among only 12 cores <250 m apart in the central and eastern parts of Botts marsh. Although the contact is sharp in six of the cores, thin beds of muddy peat alternate with mud and peaty mud above and below the contact suggesting fluctuating marsh environments rather than many decimeters of sudden tidal flooding during coseismic subsidence. Samples above and below the contact in two adjacent Russian core segments (1 m apart) are largely devoid of foraminifera, probably because they record primarily freshwater environments. The maximum-age probability distribution for contact E significantly overlaps with the distributions for nine sites on **Figure 9**, but at all but two of the sites the overlap with the distribution for contact D is greater and so a correlation with contact D is more likely than with contact E. The absence of a strong correlation of contact E's peak with any pre-1600-BP peaks for earthquake contacts at other sites is consistent with a local rather than regional change in RSL across contact E.

Conclusions

The lateral extent of sharp peat-mud contacts in cores and outcrops, coseismic subsidence evaluated with fossil diatom assemblages and reconstructed with fossil foraminiferal faunas, and correlations using ^{14}C-based age models (four of the criteria of Nelson, Shennan & Long 1996, and Shennan, Garrett & Barlow 2016) provide evidence of only three great megathrust earthquakes during the past 2000 years at the Nehalem River estuary. A peat-mud contact marking subsidence in 1700 CE, sometimes overlain by tsunami-deposited sand, can be traced over distances as great as 7 km throughout the lower estuary. Stratigraphic evidence for two earlier earthquakes, marked by peat-mud contacts B and D, is much less extensive than that for the 1700 CE earthquake and its tsunami. From 2–16 mm of silty sand above contact B in a few cores we infer that its earthquake may have been shortly followed by a tsunami. Peat-mud contacts marking coseismic subsidence during the two earlier earthquakes were found only in a 700-m by 270-m tidal marsh near the mouth of the river, where they extend for hundreds of meters. Although some other Cascadia coastal studies report evidence for an earthquake between contacts B and D, we found no extensive evidence for such an earthquake at Nehalem. The lack of evidence, except at the formerly well exposed East Bank outcrop, may be due to the complexities of preserving identifiable evidence of older earthquakes in the rapidly shifting shoreline environments of the lower river and bay. Radiocarbon ages, however, suggest that contacts B and D correlate with two of three buried, riverbank A horizons mapped by Grant (unpublished 1994 report in Supplementary Files) 5.3 km upriver. A fifth contact, E, is much less extensive and more variable in sharpness than younger contacts. The lack of foraminifera across contact E suggests that it marks a rapid local change in tidal and freshwater environments rather than RSL rise caused by regional subsidence during a great earthquake.

From changes in diatom assemblages across contacts A and B in a vibracore (V1) at the East Bank outcrop, and changes in foraminiferal assemblages across contacts A and B in the vibracore, and contacts B and D in a Botts marsh core (R5), we infer 0.7–1 m of subsidence during the three earthquakes. Quantitative reconstructions of the rapid submergence marked by the three contacts using a Bayesian foraminiferal transfer function provide the following estimates of coseismic subsidence: contact A, 1.1 ± 0.5 m (core V1); contact B, 0.7 ± 0.4 m (core V1) and 1.0 m ± 0.4 m (core R5); and contact D, 1.0 m ± 0.4 m (core R5).

The few and highly variable measures of subsidence at other central Cascadia coastal sites—and recent geophysical modeling of variable megathrust slip during the long rupture in 1700 CE—limit conclusions about rupture length and earthquake magnitude for the three Nehalem earthquakes. The 0.7–1.0 m of subsidence measured across contacts A, B, and D was likely produced by rupture of many hundreds of kilometers of the subduction zone during individual earthquakes. Much smaller subsidence measured across these contacts using non-Bayesian

transfer functions at sites in central Cascadia is better explained by patches of variable slip along the megathrust (Wang et al. 2013; Kemp et al. 2018) rather than by shorter ruptures during serial earthquakes hours to decades apart. Estimated earthquake magnitude in 1700 CE based on modeling the tsunami in Japan, and the ^{14}C dating of the rings of trees killed by coseismic subsidence in 1700 CE at sites 900 km apart (Nelson et al. 1995), makes short, serial earthquake ruptures for contact A unlikely, but the 1700 CE evidence says little about the possibility of short ruptures at the times of contacts B and D.

As with subsidence data, regional correlation of subsidence contacts based on the degree of overlap of their modeled radiocarbon-age probability distributions (**Figure 9**) is consistent with contacts A, B, and D recording earthquakes that ruptured many hundreds of kilometers of the subduction zone in 1700 CE, and about 942–764 cal a BP and 1568–1361 cal a BP, respectively. Neither measured subsidence nor comparison of modeled ^{14}C-age distributions can conclusively distinguish between long and short ruptures for the three great earthquake contacts at the Nehalem River estuary.

Supplementary Files

The Supplementary Files for this paper (at https://doi.org/10.7910/DVN/UCGUU3) include the following detailed information and data for sites described in the paper that are not summarized elsewhere. The introduction and explanation of the Supplementary Files can be found in an introductory pdf file (Part 1, Nelson et al. – Supplemental Files – Introduction, Figure captions, elevations, ^{14}C added variance, OxCal age models, references), readable with Adobe Reader 8 and higher. This introductory pdf file also includes the captions (Part 2) for the additional figures, which are included as a separate supplementary pdf file (Part 3, Nelson et al. – Supplementary Files – Figures), the methods used to determine sampling and core elevations (Part 4), the explanation of variance added to radiocarbon age errors (Part 5), and the listing of code for selected OxCal radiocarbon age models (Part 6) used in the paper. An historically important, unpublished report by Grant (1994) is a separate pdf file (Part 7, Nelson et al. – Supplementary File – Grant 1994 – unpublished MS degree report on earthquake stratigraphy of Salmon and Nehalem rivers 8Nov94.pdf). The three tables of micropaleontologic data are also separate Excel files (Part 8, Nelson et al. – Table S1 Foraminiferal data and reconstructions. xlsx; Part 8, Nelson et al. – Table S2. Total diatom valves counted in core V1.xlsx; Part 8, Nelson et al. – Table S3. Diatom species abundance for most common species in core V1.xlsx). References cited in captions for the figures and elsewhere in the Supplementary File are listed under References Cited at the end of the introductory pdf file (Part 1, Nelson et al. – Supplemental Files – Introduction, Figure captions, elevations, ^{14}C added variance, OxCal age models, references).

Acknowledgements

This work was supported by the Earthquake Hazards Program of the U.S. Geological Survey (USGS) and by NSF grants EAR-1419846, EAR-1419844, and EAR-1419824 to Hawkes, Engelhart, and Horton, respectively. Able field assistance was provided by Rich Briggs (USGS, Golden, Colorado), Zeb Maharrey (USGS, Golden, Colorado), Candice Grand Pre (University of Pennsylvania), SeanPaul La Selle (USGS, Santa Cruz, California), and J. Scott Padgett (University of Rhode Island). Some field equipment was supplied by the State of Oregon Department of Geology and Mineral Industries. Collection and preparation of diatom samples by Sawai were supported by the Geological Survey of Japan and a Japan Society for the Promotion of Science postdoctoral fellowship for research abroad. Brian Atwater (USGS, Seattle, Washington) guided Grant's work (non-thesis M.S. degree, University of Washington, Seattle, 1992) in the Nehalem River estuary (1987–1994). The National Ocean Sciences Accelerator Mass Spectrometry facility (NOSAMS) at Woods Hole Oceanographic Institution (WHOI; Woods Hole, Massachusetts) supported the analysis of four AMS ^{14}C samples during Hawkes' WHOI NOSAMS postdoctoral fellowship. Jamie Delano (USGS, Golden, Colorado), Zeb Maharrey, and Nadine Reitman helped with graphics. We thank Brian Atwater for notes from a 1997 visit to the East Bank outcrop, and for comments on an earlier version of the paper. This version of the paper, which is a contribution to IGCP Project 639 "Sea-Level Changes from Minutes to Millennia," was also improved through the suggestions of Andrew Kemp, Ian Hutchinson, and an anonymous reviewer.

Competing Interests

Simon Engelhart is a guest editor for this special collection but was removed from all editorial duties for this submission. The other authors declare that they have no competing interests.

References

Atwater, BF. 1987. Evidence for great Holocene earthquakes along the outer coast of Washington state. *Science*, 236: 942–944. DOI: https://doi.org/10.1126/science.236.4804.942

Atwater, BF. 1992. Geologic evidence for earthquakes during the past 2000 years along the Copalis River, southern coastal Washington. *Journal of Geophysical Research*, 97(B2): 1901–1919. DOI: https://doi.org/10.1029/91JB02346

Atwater, BF, Carson, B, Griggs, GB, Johnson, HP and **Salmi, MS.** 2014. Rethinking turbidite paleoseismology along the Cascadia subduction margin. *Geology*, 42: 827–830. DOI: https://doi.org/10.1130/G35902.1

Atwater, BF and **Griggs, GB.** 2012. Deep-sea turbidites as guides to Holocene earthquake history at the Cascadia subduction zone—Alternative views for a seismic-hazard workshop. *U.S. Geological Survey Open-File Report 2012–1043*, 58. DOI: https://doi.org/10.3133/ofr20121043

Atwater, BF and **Hemphill-Haley, E.** 1997. Recurrence intervals for great earthquakes of the past 3500 years at northeastern Willapa Bay, Washington. *U.S. Geological Survey Professional Paper 1576*, 108. DOI: https://doi.org/10.3133/ofr961

Atwater, BF, Musumi-Rokkaku, S, Satake, K, Tsuji, Y, Ueda, K and **Yamaguchi, DK.** 2005. The orphan tsunami of 1700—Japanese clues to a parent earthquake in North America. *U.S. Geological Survey Professional Paper 1707*, 133 p. (published jointly by University of Washington Press, Seattle). DOI: https://doi.org/10.3133/pp1707

Atwater, BF, Stuiver, M and **Yamaguchi, DK.** 1991. A radiocarbon test of earthquake magnitude at the Cascadia subduction zone. *Nature*, 353: 156–158. DOI: https://doi.org/10.1038/353156a0

Atwater, BF, Tuttle, MP, Schweig, ES, Rubin, CM, Yamaguchi, DK and **Hemphill-Haley, E.** 2004. Earthquake recurrence inferred from paleoseismology. In: Gillespie, AR, Porter, SC and Atwater, BF (eds.), *The Quaternary period in the United States, Developments in Quaternary science*, 331–350. New York: Elsevier. DOI: https://doi.org/10.1016/S1571-0866(03)01015-7

Briggs, RW, Engelhart, SE, Nelson, AR, Dura, T, Kemp, AC, Haeussler, PJ, Corbett, DR, Angster, SJ and **Bradley, L-A.** 2014. Uplift and subsidence reveal a non-persistent megathrust rupture boundary, Sitkinak Island, Alaska. *Geophysical Research Letters*, 41: 2289–2296. DOI: https://doi.org/10.1002/2014GL059380

Bronk Ramsey, C. 2001. Development of the radiocarbon program OxCal. *Radiocarbon*, 43: 355–363. DOI: https://doi.org/10.1017/S0033822200038212

Bronk Ramsey, C. 2008. Depositional models for chronological records. *Quaternary Science Reviews*, 27: 42–60. DOI: https://doi.org/10.1016/j.quascirev.2007.01.019

Bronk Ramsey, C. 2009. Bayesian analysis of radiocarbon dates. *Radiocarbon*, 51: 337–360. DOI: https://doi.org/10.1017/S0033822200033865

Bronk Ramsey, C. 2015. Radiocarbon dating in paleoseismology. In: Beer, M, et al. (eds.), *Encyclopedia of Earthquake Engineering*, 2021–2031. DOI: https://doi.org/10.1007/978-3-642-35344-4_34

Cahill, N, Kemp, AC, Parnell, AC and **Horton, BP.** 2016. A Bayesian hierarchical model for reconstructing relative sea level: from raw data to rates. *Climate of the Past*, 12: 525–542. DOI: https://doi.org/10.5194/cp-12-525-2016

Clague, JJ. 1997. Evidence for large earthquakes at the Cascadia subduction zone. *Reviews of Geophysics*, 35: 439–460. DOI: https://doi.org/10.1029/97RG00222

Clarke, SH, Jr and **Carver, GA.** 1992. Late Holocene tectonics and paleoseismicity, southern Cascadia subduction zone. *Science*, 255: 188–192. DOI: https://doi.org/10.1126/science.255.5041.188

Connolly, TJ and **Byram, S.** 1997. Oregon wet site basketry: A review of structural types. In: Oetting, AC (ed.), *Contributions to the archaeology of Oregon 1995–1997*. Association of Oregon Archaeologists Occasional Papers No. 6: 185–204.

Darienzo, ME, Peterson, CD and **Clough, C.** 1994. Stratigraphic evidence for great subduction-zone earthquakes at four estuaries in northern Oregon, U.S.A. *Journal of Coastal Research*, 10: 850–876.

de Rijk, S. 1995. Salinity control on the distribution of salt marsh foraminifera, Great Marshes, Massachusetts. *Journal of Foraminiferal Research*, 25: 156–166. DOI: https://doi.org/10.2113/gsjfr.25.2.156

Dura, T, Engelhart, SE, Vacchi, M, Horton, BP, Kopp, RE, Peltier, WR and **Bradley, S.** 2016a. The role of Holocene relative sea-level change in preserving records of subduction zone earthquakes. *Current Climate Change Reports*, 2(3): 86–100. DOI: https://doi.org/10.1007/s40641-016-0041-y

Dura, T, Hemphill-Haley, E, Sawai, Y and **Horton, BP.** 2016b. The application of diatoms to reconstruct the history of subduction zone earthquakes and tsunamis. *Earth-Science Reviews*, 152: 181–197. DOI: https://doi.org/10.1016/j.earscirev.2015.11.017

DuRoss, CB, Personius, SF, Crone, AJ, Olig, SS and **Lund, WR.** 2011. Integration of paleoseismic data from multiple sites to develop an objective earthquake chronology: application to the Weber segment of the Wasatch fault zone, Utah. *Bulletin of Seismological Society of America*, 101: 2765–2781. DOI: https://doi.org/10.1785/0120110102

Eilers, HP. 1976. The ecological biogeography of an Oregon coastal salt marsh. *Association of Pacific Coast Geographers Yearbook*, 38: 19–32. DOI: https://doi.org/10.1353/pcg.1976.0011

Engelhart, SE, Horton, BP, Nelson, AR, Hawkes, AD, Witter, RC, Wang, K, Wang, P-L and **Vane, CH.** 2013b. Testing the use of microfossils to recon-struct great earthquakes at Cascadia. *Geology*, 41: 1067–1070. DOI: https://doi.org/10.1130/G34544.1

Engelhart, SE, Horton, BP, Vane, CH, Nelson, AR, Witter, RC, Brody, SR and **Hawkes, AD.** 2013a. Modern foraminifera, $\delta^{13}C$, and bulk geochemistry of central Oregon tidal marshes and their application in paleoseismology. *Palaeogeography, Palaeoclimatology, Palaeoecology*, 377: 13–27. DOI: https://doi.org/10.1016/j.palaeo.2013.02.032

Engelhart, SE, Vacchi, M, Horton, BP, Nelson, AR and **Kopp, RE.** 2015. A sea-level database for the Pacific coast of central North America. *Quaternary Science Reviews*, 113: 78–92. DOI: https://doi.org/10.1016/j.quascirev.2014.12.001

Gilbert, JJ. 1875. Coast of Oregon between latitudes 45° 45′ and 45° 38′ including mouth of Nehalem River surveyed Aug. 25th to Sept. 11th 1875: scale 1:10,000. https://nosimagery.noaa.gov/images/shoreline_surveys/survey_scans/T-1416B.JPG.

Goldfinger, C, Galer, SG, Beeson, J, Hamilton, T, Black, B, Romos, B, Patton, J, Nelson, CH, Hausmann, R and **Morey, A.** 2016. The importance of site selection, sediment supply, and hydrodynamics: A case study of submarine paleoseismology on the northern Cascadia margin, Washington, USA. *Marine Geology*. DOI: https://doi.org/10.1016/j.margeo.2016.06.008

Goldfinger, C, Nelson, CH, Morey, A, Johnson, JE, Gutierrez-Pastor, J, Eriksson, AT, Karabanov, E, Patton, J, Gracia, E, Enkin, R, Dallimore, A, Dunhill, G and **Vallier, T.** 2012. Turbidite event history: Methods and implications for Holocene paleoseismicity of the Cascadia subduction zone. *USGS Professional Paper 1661-F*, 184 p. DOI: https://doi.org/10.3133/pp1661F

Graehl, NA, Kelsey, HM, Witter, RC, Hemphill-Haley, E and **Engelhart, SE.** 2014. Stratigraphic and microfossil evidence for a 4500-year history of Cascadia subduction zone earthquakes and tsunamis at Yaquina River estuary, Oregon, USA. *Geological Society of America Bulletin*, 127: 211–226. DOI: https://doi.org/10.1130/B31074.1

Grant, WC. 1989. More evidence from tidal-marsh stratigraphy for multiple late Holocene subduction earthquakes along the northern Oregon coast. *Geological Society of America Abstracts with Programs*, 21(5): 86.

Grant, WC, Atwater, BF, Carver, GA, Darienzo, ME, Nelson, AR, Peterson, CD and **Vick, GS.** 1989. Radiocarbon dating of late Holocene coastal subsidence above the Cascadia subduction zone— Compilation for Washington, Oregon, and northern California. *EOS*, 70(43): 1331.

Grant, WC and **McLaren, DD.** 1987. Evidence for Holocene subduction earthquakes along the northern Oregon coast. *EOS*, 68(44): 1239.

Guilbault, J-P, Clague, JJ and **Lapointe, M.** 1995. Amount of subsidence during a late Holocene earthquake—Evidence from fossil tidal marsh foraminifera at Vancouver Island, west coast of Canada. *Palaeogeography, Palaeoclimatology, Palaeoecology*, 118: 49–71. DOI: https://doi.org/10.1016/0031-0182(94)00135-U

Guilbault, J-P, Clague, JJ and **Lapointe, M.** 1996. Foraminiferal evidence for the amount of coseismic subsidence during a late Holocene earthquake on Vancouver Island, west coast of Canada. *Quaternary Science Reviews*, 15: 913–937. DOI: https://doi.org/10.1016/S0277-3791(96)00058-3

Hagstrum, JT, Atwater, BF and **Sherrod, BL.** 2004. Paleomagnetic correlation of late Holocene earthquakes among estuaries in Washington and Oregon. *Geochemistry, Geophysics, Geosystems*, 5(10): 18. DOI: https://doi.org/10.1029/2004GC000736

Hawkes, AD, Horton, BP, Nelson, AR and **Hill, DF.** 2010. The application of intertidal foraminifera to reconstruct coastal subsidence during the giant Cascadia earthquake of 1700 CE in Oregon, USA. *Quaternary International*, 122: 116–140. DOI: https://doi.org/10.1016/j.quaint.2009.09.019

Hawkes, AD, Horton, BP, Nelson, AR, Vane, CH and **Sawai, Y.** 2011. Coastal subsidence in Oregon, USA, during the giant Cascadia earthquake of 1700 CE. *Quaternary Science Reviews*, 30: 364–376. DOI: https://doi.org/10.1016/j.quascirev.2010.11.017

Hawkes, AD, Scott, DB, Lipps, JH and **Combellick, R.** 2005. Evidence for possible precursor events of megathrust earthquakes on the west coast of North America. *Geological Society of America Bulletin*, 117: 996–1008. DOI: https://doi.org/10.1130/B25455.1

Hemphill-Haley, E. 1995. Diatom evidence for earthquake-induced subsidence and tsunami 300 yr ago in southern coastal Washington. *Geological Society of America Bulletin*, 107: 367–378.

Hong, I. 2019. Developing proxies to reconstruct the intensity and magnitude of prehistoric tropical cyclones and earthquakes, *PhD dissertation*, Department of Marine and Coastal Studies, Rutgers University, New Brunswick, New Jersey, 183.

Horton, BP and **Edwards, BP.** 2006. Quantifying Holocene sea-level change using intertidal foraminifera: lessons from the British Isles. *Cushman Foundation for Foraminiferal Research, Special Publication No. 40*, 97.

Horton, BP, Milker, Y, Dura, T, Wang, K, Bridgeland, WT, Brophy, L, Ewald, M, Khan, NS, Engelhart, SE, Nelson, AR and **Witter, RC.** 2017. Microfossil measures of rapid sea-level rise: Timing of response of two microfossil groups to a sudden tidal-flooding experiment in Cascadia. *Geology*. DOI: https://doi.org/10.1130/G38832.1

Horton, BP, Zong, Y, Hillier, C and **Engelhart, S.** 2007. Diatoms from Indonesian mangroves and their suitability as sea-level indicators for tropical environments. *Marine Micropaleontology*, 63: 155–168. DOI: https://doi.org/10.1016/j.marmicro.2006.11.005

Hutchinson, I and **Clague, JJ.** 2017. Were they all giants? Perspectives on late Holocene plate-boundary earthquakes at the northern end of the Cascadia subduction zone. *Quaternary Science Reviews*, 169: 29–49. DOI: https://doi.org/10.1016/j.quascirev.2017.05.015

Hutchinson, I, Guilbault, J-P, Clague, JJ and **Bobrowsky, PT.** 2000. Tsunamis and tectonic deformation at the northern Cascadia margin: a 3000-year record from Deserted Lake, Vancouver Island, British Columbia. *The Holocene*, 10: 429–439. DOI: https://doi.org/10.1191/095968300666654539

Janousek, CN and **Folger, CL.** 2014. Variation in tidal wetland plant diversity and composition within and among coastal estuaries: assessing the relative importance of environmental gradients. *Journal of Vegetation Science*, 25: 534–545. DOI: https://doi.org/10.1111/jvs.12107

Johannessen, CL. 1961. Chapter 7. Shoreline and vegetation changes of the estuaries. In: Dicken, SN (ed.), *Some recent physical changes of the Oregon coast: Report on an investigation for the Office of Naval Research* (Contract Nonr-2771(04), Project NR 388-062): 100–138. Eugene, Oregon: U.S. Department of the Navy and Department of Geography, University of Oregon.

Kelsey, HM, Nelson, AR, Hemphill-Haley, E and **Witter, R.** 2005. Tsunami history of an Oregon coastal lake reveals a 4600 yr record of great earthquakes on the Cascadia subduction zone. *Geological Society of America Bulletin*, 117: 1009–1032. DOI: https://doi.org/10.1130/B25452.1

Kelsey, HM, Witter, RC and **Hemphill-Haley, E.** 1998. Response of a small Oregon estuary to coseismic subsidence and postseismic uplift in the past 300 years. *Geology*, 26: 231–234. DOI: https://doi.org/10.1130/0091-7613(1998)026<0231:ROASOE>2.3.CO;2

Kelsey, HM, Witter, RC and **Hemphill-Haley, E.** 2002. Plate-boundary earthquakes and tsunamis of the past 5500 years, Sixes River estuary, southern Oregon. *Geological Society of America Bulletin*, 114: 298–314. DOI: https://doi.org/10.1130/0016-7606(2002)114<0298:PBEATO>2.0.CO;2

Kemp, AC, Cahill, N, Engelhart, SE, Hawkes, AD and **Wang, K.** 2018. Revising estimates of spatially variable subsidence during the 1700 CE Cascadia earthquake using a Bayesian foraminiferal transfer function. *Bulletin of Seismological Society of America*, 108(2): 654–673. DOI: https://doi.org/10.1785/0120170269

Kemp, AC, Horton, BP, Corbett, DR, Culver, SJ, Edwards, RJ and **van de Plassche, O.** 2009. The relative utility of foraminifera and diatoms for reconstructing late Holocene sea-level change in North Carolina, USA. *Quaternary Research*, 71: 9–21. DOI: https://doi.org/10.1016/j.yqres.2008.08.007

Kemp, AC, Nelson, AR and **Horton, BP.** 2013. Radiocarbon dating of plant macrofossils in tidal marsh sediment. In: Schroder, J (ed.), *Treatise on Geomorphology*, 370–388. San Diego, CA: Academic Press. DOI: https://doi.org/10.1016/B978-0-12-374739-6.00400-0

Kemp, AC and **Telford, RJ.** 2015. Transfer Functions. In: Shennan, I, Long, AJ and Horton, BP (eds.), *Handbook of Sea-Level Research*, chapter 31: 470–499. Chichester, UK: Wiley-Blackwell. DOI: https://doi.org/10.1002/9781118452547.ch31

Leonard, LJ, Currie, CA, Mazzotti, S and **Hyndman, RD.** 2010. Rupture area and displacement of past Cascadia great earthquakes from coastal coseismic subsidence. *Geological Society of America Bulletin,* 122: 1951–1968. DOI: https://doi.org/10.1130/B30108.1

Losey, RJ. 2002. Communities and Catastrophe: Tillamook response to the 1700 CE earthquake and tsunami, northern Oregon coast [*Ph.D. dissertation*]: Eugene, Oregon: Department of Anthropology, University of Oregon, 636.

Losey, RJ. 2005. Earthquakes and tsunami as elements of environmental disturbance on the northwest coast of North America. *Journal of Anthropological Archaeology*, 24: 101–116. DOI: https://doi.org/10.1016/j.jaa.2005.02.001

Losey, RJ, Erlandson, JM and **Moss, ML.** 2000. Assessing the impacts of Cascadia subduction zone earthquakes on the people and landscapes of the Northwest Coast: Methodological issues and case studies from the northern Oregon coast. In: Losey, RJ (ed.), *Changing Landscapes, Proceedings of the 3rd Annual Coquille Cultural Preservation Conference, 1999*, 124–142. North Bend, Oregon: Coquille Indian Tribe.

Milker, Y, Horton, BP, Nelson, AR, Engelhart, SE and **Witter, RC.** 2015b. Variability of intertidal foraminiferal assemblages in a salt marsh, Oregon, USA. *Marine Micropaleontology*, 118: 1–16. DOI: https://doi.org/10.1016/j.marmicro.2015.04.004

Milker, Y, Horton, BP, Vane, CH, Engelhart, SE, Nelson, AR, Witter, RC, Khan, NS and **Bridgeland, WT.** 2015a. Annual and seasonal distribution of intertidal foraminifera and stable carbon isotope geochemistry, Bandon Marsh, Oregon, USA. *Journal of Foraminiferal Research*, 45: 146–155. DOI: https://doi.org/10.2113/gsjfr.45.2.146

Milker, Y, Nelson, AR, Horton, BP, Engelhart, SE, Bradley, L-A and **Witter, RC.** 2016. Differences in coastal subsidence in southern Oregon (USA) during at least six prehistoric megathrust earthquakes. *Quaternary Science Reviews*, 142: 143–163. DOI: https://doi.org/10.1016/j.quascirev.2016.04.017

Minor, R. 1991. Archaeology of the Nehalem Bay dune site, northern Oregon coast. *Report 2018 to the Oregon State Historic Preservation Office, Department of Parks and Recreation*, Salem, Oregon.

Minor, R and **Grant, WC.** 1996. Earthquake-induced subsidence and burial of late Holocene archaeological sites, northern Oregon coast. *American Antiquity*, 61(4): 772–781. DOI: https://doi.org/10.2307/282017

Minor, R and **Peterson, CD.** 2016. Multiple reoccupations after four paleotsunami inundations (0.3–1.3 ka) at a prehistoric site in the Netarts littoral cell, northern Oregon coast, USA. *Geoarchaeology*, 32(2): 248–266. DOI: https://doi.org/10.1002/gea.21593

Molino, G, Wheatcroft, R, Peck, E and **Brophy, L.** 2016. *Anthropogenic causes of accelerated sediment accumulation, rates in Nehalem Bay salt marshes, Oregon.* American Geophysical Union, Fall General Assembly, abstract #EP21B-0881.

Moss, ML and **Erlandson, JM.** 1995. An evaluation, survey and dating program for archaeological sites on state lands of the northern Oregon coast. *Department of Anthropology, University of Oregon, Eugene, report to the Oregon State Historic Preservation Office, Department of Parks and Recreation*, Salem, Oregon.

Nelson, AR. 1992a. Holocene tidal-marsh stratigraphy in south-central Oregon—Evidence for localized sudden submergence in the Cascadia subduction zone. In: Fletcher, CP and Wehmiller, JF (eds.), *Quaternary coasts of the United States—Marine and lacustrine systems*, 287–301. Tulsa, Oklahoma: Society for Sedimentary Geology Special Publication 48. DOI: https://doi.org/10.2110/pec.92.48.0287

Nelson, AR. 1992b. Discordant ^{14}C ages from buried tidal-marsh soils in the Cascadia subduction zone, southern Oregon coast. *Quaternary Research*, 38: 74–90. DOI: https://doi.org/10.1016/0033-5894(92)90031-D

Nelson, AR. 2015. Chapter 4: *Coastal sediment.* In: Shennan, I, Long, AJ and Horton, BP (eds.), *Handbook of Sea-level Research*, 218–272. Chichester: Wiley-Blackwell.

Nelson, AR, Asquith, AC and **Grant, WC.** 2004. Great earthquakes and tsunamis of the past 2000 years at the Salmon River estuary, central Oregon coast, USA. *Bulletin of Seismological Society of America*, 94: 1276–1292. DOI: https://doi.org/10.1785/012003210

Nelson, AR, Atwater, BF, Bobrowsky, PT, Bradley, L-A, Clague, JJ, Carver, GA, Darienzo, ME, Grant, WC, Krueger, HW, Sparks, R, Stafford, TW, Jr and **Stuiver, M.** 1995. Radiocarbon evidence for extensive plate-boundary rupture about 300 years ago at the Cascadia subduction zone. *Nature*, 378: 371–374. DOI: https://doi.org/10.1038/378371a0

Nelson, AR, Jennings, AE and **Kashima, K.** 1996. An earthquake history derived from stratigraphic and microfossil evidence of relative sea-level change at Coos Bay, southern coastal Oregon. *Geological Society of America Bulletin*, 108: 141–154. DOI: https://doi.org/10.1130/0016-7606(1996)108<0141:AEHDFS>2.3.CO;2

Nelson, AR, Kelsey, HM and **Witter, RC.** 2006. Great earthquakes of variable magnitude at the Cascadia subduction zone. *Quaternary Research*, 65: 354–365. DOI: https://doi.org/10.1016/j.yqres.2006.02.009

Nelson, AR, Ota, Y, Umitsu, M, Kashima, K and **Matshushima, Y.** 1998. Seismic or hydrodynamic control of rapid late-Holocene sea-level rise in southern coastal Oregon, USA? *The Holocene*, 8: 287–299. DOI: https://doi.org/10.1191/095968398668600476

Nelson, AR and **Personius, SF.** 1996. Great-earthquake potential in Oregon and Washington—An overview of recent coastal geologic studies and their bearing on segmentation of Holocene ruptures, central Cascadia subduction zone. In: Rogers, AM, Walsh, TJ, Kockelman, WJ and Priest, GR (eds.), *Assessing earthquake hazards and reducing risk in the Pacific Northwest*, 91–114. U.S. Geological Survey Professional Paper 1560.

Nelson, AR, Personius, SF, Sherrod, BL, Kelsey, HM, Johnson, SY, Bradley, L-A and **Wells, RE.** 2014. Diverse rupture modes for surface-deforming upper plate earthquakes in the southern Puget Lowland of Washington State. *Geosphere*, 10: 769–796. DOI: https://doi.org/10.1130/GES00967.1

Nelson, AR, Sawai, Y, Jennings, A, Bradley, L, Sherrod, B, Sabean, J and **Horton, BP.** 2008. Great-earthquake paleogeodesy and tsunamis of the past 2000 years at Alsea Bay, central Oregon coast, USA. *Quaternary Science Reviews*, 27: 747–768. DOI: https://doi.org/10.1016/j.quascirev.2008.01.001

Nelson, AR, Shennan, I and **Long, AJ.** 1996. Identifying coseismic subsidence in tidal-wetland stratigraphic sequences at the Cascadia subduction zone of western North America. *Journal of Geophysical Research*, 101(B3): 6115–6135. DOI: https://doi.org/10.1029/95JB01051

Padgett, JS. 2019. Cascadia subduction zone coseismic subsidence estimates from northern California and Washington, PhD dissertation. Kingston, Rhode Island: Department of Geosciences, The University of Rhode Island, 176 pp.

Peterson, CD, Cruikshank, KM, Schlichting, RB and **Braunsten, S.** 2010. Distal runup records of latest Holocene paleotsunami in alluvial flood plains: Neskowin and Beaver Creek, Oregon, central Cascadia margin, U.S. *Journal of Coastal Research*, 26: 622–634. DOI: https://doi.org/10.2112/08-1147.1

Reimer, PJ, Bard, E, Bayliss, A, Beck, JW, Blackwell, PG, Bronk Ramsey, C, Grootes, PM, Guilderson, TP, Haflidason, H, Hajdas, I, Hatté, C, Heaton, TJ, Hoffmann, DL, Hogg, AG, Hughen, KA, Kaiser, KF, Kromer, B, Manning, SW, Niu, M, Reimer, RW, Richards, DA, Scott, EM, Southon, JR, Staff, RA, Turney, CSM and **van der Plicht, J.** 2013. IntCal13 and Marine13 radiocarbon age calibration curves 0–50,000 years cal BP. *Radiocarbon*, 55: 1869–1887. DOI: https://doi.org/10.2458/azu_js_rc.55.16947

Sabean, J. 2004. Application of foraminifera to detecting land level change associated with great earthquakes along the west coast of North America [unpublished M.S, thesis]. Vancouver, Canada: Department of Earth Sciences, Simon Fraser University, 85.

Satake, K, Shimazaki, K, Tsuji, Y and **Ueda, K.** 1996. Time and size of a giant earthquake in Cascadia inferred from Japanese tsunami records of January 1700. *Nature*, 379: 246–249. DOI: https://doi.org/10.1038/379246a0

Satake, K, Wang, K and **Atwater, BF.** 2003. Fault slip and seismic moment of the 1700 Cascadia earthquake inferred from Japanese tsunami descriptions. *Journal of Geophysical Research*, 108(B11): 2535. DOI: https://doi.org/10.1029/2003JB002521

Sawai, Y. 2001. Distribution of living and dead diatoms in tidal wetlands of northern Japan: relations to taphonomy. *Palaeogeography, Palaeoclimatology, Palaeoecology*, 173: 125–141. DOI: https://doi.org/10.1016/S0031-0182(01)00313-3

Sawai, Y, Horton, BE, Kemp, AC, Hawkes, AD, Nagumo, T and **Nelson, AR.** 2016a. Relations among diatoms and tidal environments in Oregon and Washington, USA. *Diatom Research*, 31(1): 17–38. DOI: https://doi.org/10.1080/0269249X.2015.1126359

Sawai, Y and **Nagumo, T.** 2003. Diatoms from Alsea Bay, Oregon, USA. *Diatom*, 19: 33–46.

Sawai, Y, Nagumo, T and **Nelson, AR.** 2016b. A brackish diatom, *Pseudofrustulia lancea* gen. et sp. Nov. (Bacillariophyceae), from the Pacific Coast of Oregon (USA). *Phytotaxa*, 267: 103–112. DOI: https://doi.org/10.11646/phytotaxa.267.2.2

Sawai, Y, Nasu, H and **Yasuda, Y.** 2002. Fluctuations in relative sea-level during the past 3000 yr in the Onneth estuary, Hokkaido, northern Japan. *Journal of Quaternary Science*, 17(5–6): 607–622. DOI: https://doi.org/10.1002/jqs.708

Scheans, D, Churchill, T, Stenger, A and **Hajda, Y.** 1990. *Summary report on the 1989 excavations at the Cronin Point Site (35-TI-4B), Nehalem State Park, Oregon.* Portland, Oregon: Institute for Archaeological Studies.

Schlichting, RB and **Peterson, CD.** 2006. Mapped overland distance of paleotsunami high-velocity inundation in back-barrier wetlands of the central Cascadia margin, USA. *Journal of Geology*, 114: 577–592. DOI: https://doi.org/10.1086/506164

Scott, DB and **Hermelin, JOR.** 1993. A device for precision splitting of micropaleontological samples in liquid suspension. *Journal of Paleontology*, 67: 151–154. DOI: https://doi.org/10.1017/S0022336000021302

Shennan, I, Bruhn, R, Barlow, N, Good, K and **Hocking, E.** 2014. Late Holocene great earthquakes in the eastern part of the Aleutian megathrust. *Quaternary Science Reviews*. DOI: https://doi.org/10.1016/j.quascirev.2013.11.010

Shennan, I, Garrett, E and **Barlow, N.** 2016. Detection limits of tidal-wetland sequences to identify variable rupture modes of megathrust earthquakes. *Quaternary Science Reviews*. DOI: https://doi.org/10.1016/j.quascirev.2016.08.003

Shennan, I, Long, AJ, Rutherford, MM, Green, FM, Innes, JB, Lloyd, JM, Zong, Y and **Walker, KJ.** 1996. Tidal marsh stratigraphy, sea-level change and large earthquakes, I: A 5000 year record in Washington, USA. *Quaternary Science Reviews*, 15: 1023–1059. DOI: https://doi.org/10.1016/S0277-3791(96)00007-8

Shennan, I, Long, AJ, Rutherford, MM, Innes, JB, Green, FM, Kirby, JR and **Walker, KJ.** 1998. Tidal marsh stratigraphy, sea-level change and large earthquakes, II: Submergence events during the last 3500 years at Netarts Bay, Oregon, USA. *Quaternary Science Reviews*, 17: 365–393. DOI: https://doi.org/10.1016/S0277-3791(97)00055-3

Taylor, RE, Stuiver, M and **Reimer, PJ.** 1996. Development and extension of the calibration of the radiocarbon time scale: Archaeological applications. *Quaternary Science Reviews,* 15: 655–668. DOI: https://doi.org/10.1016/0277-3791(96)00024-8

Troels-Smith, J. 1955. Characterization of unconsolidated sediments. *Geological Survey of Denmark, Series IV*, 3(10): 39–71.

Valentine, DW, Keller, EA, Carver, GA, Li, W-H, Manhart, C and **Simms, AR.** 2012. Paleoseismicity of the southern end of the Cascadia subduction zone, northwestern California. *Bulletin of Seismological Society of America*, 102: 1059–1078. DOI: https://doi.org/10.1785/0120110103

Wang, P-L, Engelhart, SE, Wang, K, Hawkes, AD, Horton, BP, Nelson, AR and **Witter, RC.** 2013. Heterogeneous rupture in the great Cascadia earthquake of 1700 inferred from coastal subsidence estimates. *Journal of Geophysical Research–Solid Earth*, 118. DOI: https://doi.org/10.1002/jgrb.50101

Ward, GK and **Wilson, SR.** 1978. Procedures for comparing and combining radiocarbon age determinations: A critique. *Archaeometry*, 20:19–31. DOI: https://doi.org/10.1111/j.1475-4754.1978.tb00208.x

Witter, RC, Hemphill-Haley, E, Hart, R and **Gay, L.** 2009. Tracking Prehistoric Cascadia Tsunami Deposits at Nestucca Bay, Oregon. U.S. Geological Survey, National Earthquake Hazards Reduction Program Final Technical Report 08HQGR0076, 92 p.

Witter, RC, Kelsey, HM and **Hemphill-Haley, E.** 2003. Great Cascadia earthquakes and tsunamis of the past 6700 years, Coquille River estuary, southern coastal Oregon. *Geological Society of America Bulletin*, 115: 1289–1306. DOI: https://doi.org/10.1130/B25189.1

Witter, RC, Zhang, YJ, Wang, K, Goldfinger, C and **Priest, GR.** 2012. Coseismic slip on the southern Cascadia megathrust implied by tsunami deposits in an Oregon lake and earthquake-triggered marine turbidites. *Journal of Geophysical Research*, 117(B10303). DOI: https://doi.org/10.1029/2012JB009404

Witter, RC, Zhang, YJ, Wang, K, Priest, GR, Goldfinger, C, Stimely, L, English, JT and **Ferro, PA.** 2013. Simulated tsunami inundation for a range of Cascadia megathrust earthquake scenarios at Bandon, Oregon, USA. *Geosphere*. DOI: https://doi.org/10.1130/GES00899.1

Woodward, J, White, J and **Cummings, R.** 1990. Paleoseismicity and the archaeological record: Areas of investigation on the northern Oregon coast. *Oregon Geology*, 52(3): 57–65.

Wright, AJ, Edwards, RJ and **van de Plassche, O.** 2011. Reassessing transfer-function performance in sea-level reconstruction based on benthic salt-marsh foraminifera from the Atlantic coast of NE North America. *Marine Micropaleontology*, 81: 43–62. DOI: https://doi.org/10.1016/j.marmicro.2011.07.003

How to cite this article: Nelson, AR, Hawkes, AD, Sawai, Y, Engelhart, SE, Witter, R, Grant-Walter, WC, Bradley, L-A, Dura, T, Cahill, N and Horton, B. 2020. Identifying the Greatest Earthquakes of the Past 2000 Years at the Nehalem River Estuary, Northern Oregon Coast, USA. *Open Quaternary*, 6: 2, pp. 1–30. DOI: https://doi.org/10.5334/oq.70

Submitted: 21 June 2019 **Accepted:** 28 October 2019 **Published:** 14 January 2020

]u[*Open Quaternary* is a peer-reviewed open access journal published by Ubiquity Press. OPEN ACCESS